

# Four Fold Angular Decay Distribution of $\Lambda_b$ Decay



By

**Rana Khan**

Reg No

**365346**

Supervisor

**Dr. Faisal Munir Bhutta**

**Department of Physics**  
SCHOOL OF NATURAL SCIENCE  
NATIONAL UNIVERSITY OF SCIENCE AND TECHNOLOGY  
ISLAMABAD.  
2024.

# **Four Fold Angular Decay Distribution of $\Lambda_b$ Decay**

By

**Rana Khan**

Reg No

**365346**

A thesis submitted in partial fulfillment of the requirements for  
the degree of

**MS Physics**

Supervisor

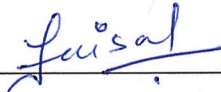
**Dr. Faisal Munir Bhutta**

Supervisor's Signature: \_\_\_\_\_

**Department of Physics**  
SCHOOL OF NATURAL SCIENCE  
NATIONAL UNIVERSITY OF SCIENCE AND TECHNOLOGY  
ISLAMABAD.  
2024.

## THESIS ACCEPTANCE CERTIFICATE

Certified that final copy of MS thesis written by **Rana Khan** (Registration No. **00000365346**), of **School of Natural Sciences** has been vetted by undersigned, found complete in all respects as per NUST statutes/regulations, is free of plagiarism, errors, and mistakes and is accepted as partial fulfillment for award of MS/M.Phil degree. It is further certified that necessary amendments as pointed out by GEC members and external examiner of the scholar have also been incorporated in the said thesis.

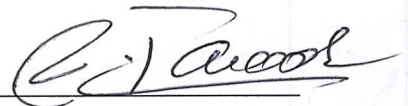
Signature: 

Name of Supervisor: Dr. Faisal Munir Bhutta

Date: 09-05-2024

Signature (HoD): 

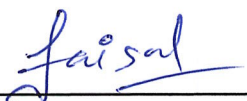

Date: 09-05-2024

Signature (Dean/Principal): 

Date: 13.5.2024

**National University of Sciences & Technology****MS THESIS WORK**

We hereby recommend that the dissertation prepared under our supervision by: Rana Khan, Regn No. 00000365346 Titled: Four Fold Angular Decay Distribution of Lambda-b Decay be Accepted in partial fulfillment of the requirements for the award of **MS** degree.

**Examination Committee Members**1. Name: DR. MUHAMMAD ALI PARACHASignature:  \_\_\_\_\_2. Name: DR. SAADI ISHAQSignature:  \_\_\_\_\_Supervisor's Name: DR. FASIAL MUNIR BHUTTASignature:  \_\_\_\_\_  
\_\_\_\_\_  
Head of Department09-05-2024  
\_\_\_\_\_  
Date**COUNTERSIGNED**Date: 13.5.2024  
\_\_\_\_\_  
Dean/Principal

## Declaration

I certify that this research work titled "Four Fold Angular Decay Distribution of  $\Lambda_b$  Decay" is my own work. The work has not been presented elsewhere for assessment. The material that has been used from other sources it has been properly acknowledged/referred.

Signature of Student  
RANA KHAN  
365346

## Abstract

This thesis addresses the semi leptonic decay process of  $\Lambda_b \rightarrow \Lambda(\rightarrow N\pi)l^+l^-$  using  $\Lambda_b$  as unpolarized baryon. The hamiltonian for the decay is derived using the framework of Operator Product Expansion (OPE) that splits the problem into short- and long-distance physics. The Standard Model (SM) operator basis are utilized along with the chirality flipped basis, which are relevant for the contribution to physics beyond the Standard Model. The four fold differential decay distribution is expressed in term of the ten angular observables. The short-distance physics is defined by Wilson coefficients, which are computed within the SM using perturbative Quantum Chromodynamics (QCD) using loop diagrams, whereas long-distance physics requires matrix elements of the local operators, which are derived using non-perturbative QCD methods, particularly lattice QCD.

We obtain the four-fold differential decay width for the process in two steps: first, by analyzing the  $\Lambda_b \rightarrow \Lambda l^+l^-$  transition, and then by studying the  $\Lambda(\rightarrow N\pi)$  decay. This hadronic matrix elements for  $\Lambda_b \rightarrow \Lambda$  and  $\Lambda \rightarrow N$  transition are defined in the helicity basis and they are written in terms of the hadronic form factors. For the later part of the decay process two independent hadronic form factors appear while for the former part of the decay ten independent form factor appear. For numerical analysis the values of the form factors are taken from the lattice QCD predictions. The new physics Wilson coefficients information is collected from current literature and the data is taken from the global fit analysis with best fit values for the vector and the axial vector scenarios of the Wilson coefficients. Finally, we predict various observables for the decay channel in both the Standard Model and the two new physics scenarios along with their comparison with the experimental predictions.

## Acknowledgments

Foremost, I am very grateful to ALLAH ALMIGHTY for the grace and blessing HE bestowed upon me and gave me the strength to finish this project.

A huge thanks to my thesis advisor Dr. Faisal Munir Bhutta for his continuous guidance, kind supervision and knowledgeable instructions that directed me to complete my MS project. I am very grateful to him for giving his valuable time to me. It was a great honor to work under his supervision. Deepest gratitude to him for their help, support, and encouragement. Without his help, I could never complete this thesis.

I am profusely thankful to my beloved parents who raised me when I was not capable of walking and continued to support me throughout in every department of my life. Finally, I would like to express my gratitude to all the individuals who have rendered valuable assistance to my study.

# Contents

List of Figures	v
List of Tables	vi
<b>1 Introduction</b>	<b>1</b>
<b>2 Theoretical Framework</b>	<b>3</b>
2.1 Effective Field Theory . . . . .	3
2.1.1 Why we use EFTs . . . . .	3
2.1.2 Basic Ingredient of EFTs . . . . .	3
2.1.3 General EFTs . . . . .	4
2.2 Beyond Standard Model . . . . .	5
2.3 Standard Model: As an EFT . . . . .	6
2.4 Flavor in the Standard Model . . . . .	6
2.5 Weak Interaction of Quarks . . . . .	9
2.5.1 Flavor Changing Neutral Current Transition . . . . .	9
2.5.2 The CKM Matrices . . . . .	10
2.5.3 GIM Mechanism . . . . .	13
2.6 Operator Product Expansion . . . . .	13
2.7 Effective Hamiltonian for FCNCs . . . . .	14
<b>3 Formalism</b>	<b>16</b>
3.1 Effective Hamiltonian . . . . .	16
3.1.1 New physics in Effective Hamiltonian . . . . .	17
3.2 Amplitude for $\Lambda_b \rightarrow \Lambda l^+ l^-$ . . . . .	17
3.2.1 Hadron Matrix Element Calculation . . . . .	19
3.2.2 Hadronic Coupling for $\Lambda(u, d, s) \rightarrow N\pi$ . . . . .	22
3.3 Four fold differential distribution in the cascade decay . . . . .	23
3.4 Observable Calculations . . . . .	25
3.4.1 Uncertainty Calculation . . . . .	26
<b>4 Numerical Analysis</b>	<b>27</b>
4.1 SM Results for $\Lambda_b \rightarrow \Lambda(\rightarrow N\pi)l^+l^-$ . . . . .	28
4.2 NP results for $\Lambda_b \rightarrow \Lambda(\rightarrow N\pi)l^+l^-$ . . . . .	34
<b>5 Conclusions</b>	<b>42</b>
<b>A Detail on the Kinematics</b>	<b>44</b>
A.1 Di-lepton rest frame . . . . .	44
A.2 $\Lambda_b$ rest frame . . . . .	44
A.3 $N\pi$ System . . . . .	46
A.4 Partial Decay Rate . . . . .	46



<b>B Leptonic Tensor</b>	<b>49</b>
<b>C Hadronic Part</b>	<b>50</b>
C.1 Hadronic Spinor Representation . . . . .	50
C.2 Hadronic Spinor Bilinears . . . . .	50
C.3 Four Fold Distribution Final Spin Orientation . . . . .	51
<b>D Related Formulae</b>	<b>53</b>
D.1 Wilson Coefficient . . . . .	53
D.2 Form Factors . . . . .	53
<b>Bibliography</b>	<b>55</b>

# List of Figures

2.1	Penguin Diagram	9
2.2	Box Diagram	10
2.3	The definition of $V_{ij}$ and $V_{ij}^*$ .	13
2.4	Penguin Diagram for FCNC $b \rightarrow sl^+l^-$	15
4.1	Differential Branching Fraction $\frac{d\beta}{dq^2}$ .	29
4.2	Longitudinal polarization fraction of di-leptons ( $F_L$ ).	30
4.3	Lepton Forward-Backward Asymmetry ( $A_{FB}^l$ ).	31
4.4	Lepton Hadron Forward Backward Asymmetry ( $A_{FB}^{l\Lambda}$ ).	32
4.5	Hadron Forward Backward Asymmetry ( $A_{FB}^\Lambda$ ).	33
4.6	SM Results for $\hat{K}_{2ss}$ , $\hat{K}_{2cc}$ , $\hat{K}_{4sc}$ , and $\hat{K}_{4s}$ .	34
4.7	NP Results for Branching Fraction $\frac{d\beta}{dq^2}$ .	36
4.8	NP Results for the Longitudinal Polarization fraction of di-Leptons ( $F_L$ ).	37
4.9	NP Results for Lepton Forward Backward Asymmetry ( $A_{FB}^l$ ).	38
4.10	NP Results for Lepton Hadron Forward Backward Asymmetry ( $A_{FB}^{l\Lambda}$ ).	39
4.11	NP Results for Hadron Forward Backward Asymmetry ( $A_{FB}^\Lambda$ ).	40
4.12	NP prediction for $\hat{K}_{2ss}$ , $\hat{K}_{2cc}$ , $\hat{K}_{4sc}$ , and $\hat{K}_{4s}$ .	41
A.1	$\Lambda_b \rightarrow \Lambda(\rightarrow N\pi)l^+l^-$ decay kinematics with $\theta_l$ , $\theta_\Lambda$ are angle between the z-axis and flight axis of Di-leptons and $N\pi$ system respectively where $\phi$ is azimuthal angle or angle between the plane of flights.	45

# List of Tables

2.1	Properties of the Standard Model quarks and leptons. . . . .	8
4.1	Values of the used input parameters. . . . .	27
4.2	Global fit values of Wilson coefficients. . . . .	35

# Chapter 1

## Introduction

The field of particle physics is study of basic elements of matter and the forces that interacts with them. By explaining the behavior of the fundamental particles of matter, this field of physics aims to provide answers to puzzles concerning the nature of the universe. The goal of particle physicists is to identify new particles and categorize them according to their characteristics. This field focus on the fundamental makeup of matter and their forces that deals with their interaction. It offers insights into the cosmos immediately following the Big Bang. Particle physics has played a crucial role in advancing our comprehension of the cosmos and its fundamental building blocks. It led physicist to the discovery of previously unknown sub atomic particles, and confirmed their validity by field theories.

Every concept we study in physics is basically a field theory. Simply stated effective field theories are quantum field theories that work upto a certain energy scale. EFT explanation may be required for a physical system if a more basic theory is absent. Sometimes it is very challenging to derive precise or even close predictions from an EFT for instant when it is highly coupled. Under these circumstances, weakly coupled EFTs can offer a more practical explanation of the same physical system. Overall, EFTs can be a useful framework even in situations where they are not necessary. EFTs significantly reduce computational difficulty by focusing on the vital degrees of freedom. By considering only the required degree of freedom it is possible for new symmetries to become apparent. In EFT the physics is divided into two parts: first, which depends on the physics we are ignoring, and second is the actual EFT calculation, which deals with the degrees of freedom we are concerned with.

Standard model of particle physics is an efficient framework to describe nature of particle and their interactions. Coming from an EFT approach standard model also work upto some energy scale. This means that SM is a right theory upto at least weak energy scale. This scale means that the energy is directly probed by the human in large hadron collider experiment. Likewise, SMEFT general structure are in particular the field, symmetry and interaction. An SMEFT is used for one scale at a time for calculation to become convenient.

Beside the field theory approach, SM itself is a gauge theory that is based on the symmetry group,

$$SU(3)_C \otimes SU(2)_L \otimes U(1)_Y. \quad (1.1)$$

$SU(3)_C$  describes strong force with 8-massless gluon, weak force is represented by  $SU(2)_L$ : with three massive boson  $W^\pm, Z^0$ , and electromagnetic is represented by  $U(1)_Y$ : with a massless photon  $\gamma$  interaction. For the past thirty years the experimental prediction has been tested in accordance with standard model theory. However, it is also considered that the SM is the tail of a more complex and wide theory.

It is very important in the field of particle physics to brings exact match between what is predicted theoretically and what is actually observed in experiments. The standard model fails to explain a variety of particle interactions, and their experimental result. We want to create a more solid theoretical framework that is more closely resembles experimental results and we

called the physics beyond the standard model. Various approaches are used to tackle the problem. For example, extension to standard model are made named as super symmetric model,  $Z'$  model, etc. Direct search is used to get any direct presence of particle in the large hadron collider experiment. Another way is the indirect search which investigate SM processes (like FCNC decay transition) and examine the role of NP in them or the effects of heavier particles can be observed. The main driving objective of our study is to exploring "new physics" in order to bring together theoretical and experimental findings. Our research tries to correct this imbalance up to a certain limit [1].

Radiative and rare semi-leptonic decays within and beyond the Standard Model (SM) can be studied through the decays of  $b \rightarrow s$  (quark-level) transition. Dileptonic flavor-changing neutral currents (FCNCs) decays like  $\Lambda_b \rightarrow \Lambda(\rightarrow N\pi)l^+l^-$  are sensitive probes of NP beyond the Standard Model (SM). The high energy effect can be appear in these FCNCs transition which will change the amplitude from the standard model prediction. Measuring their decay rates and angular distributions predictions of the SM and beyond it can be verified. Changes in the rate or angular distributions from those predicted by the Standard Model (SM) might be signs of the existence of New Physics beyond the Standard Model.

Aim of our study here is to describe the four fold angular distribution of  $\Lambda_b(u, d, b) \rightarrow \Lambda(u, d, s)(\rightarrow N\pi) \rightarrow l^+l^-$  [2] in the Standard model and effects of new physics in it. A model independent analysis is used in our decay where the chirality flipped operator are used in NP effect from the standard model part. The analysis also incorporated the wilson co-efficient information from the global fit analysis. Since the standard model cannot consistently anticipate outcomes that are consistent with experimental data, our goal is to get beyond it. The main goal of adding New Physics ideas is to improve the correlation between our results and actual evidence. The four-fold differential decay rate allows for the definition of a number of physical observable that we measured by theoretical calculation. Quark level transition such as  $b \rightarrow s$  in  $\Lambda_b \rightarrow \Lambda(\rightarrow N\pi)l^+l^-$  are thus considered as playing a vital rule to contribution of physics beyond the standard model.

The CDF collaboration recently observed the decay of  $\Lambda_b \rightarrow \Lambda\mu^+\mu^-$  with a branching ratio of order  $10^{-6}$ . In number of recent paper [2–13] SM and NP analysis of decay are presented.

The structure of this thesis consists of five main chapters that underlines the investigation of Lambda b-decays. The chapter 2 presents the idea of Effective Field Theories (EFTs), basic ingredients of EFTs, explains its importance in theoretical physics, especially for systems for which a complete theory is either unknown or too complicated to understand. A thorough examination of flavor dynamics in the Standard Model is given in this chapter, with particular attention to the mechanisms underlying Flavor-Changing Neutral Currents (FCNCs) and how they are represented in the Cabibbo-Kobayashi-Maskawa (CKM) matrix. It explores the CKM mechanism. The formalism for the decay processes of heavy baryons is provided in chapter 3. The function of helicity amplitudes and the unique contributions of hadronic elements to transitions are then discussed in this chapter. The numerical study of the Standard Model and NP decay predictions is presented in chapter 4. It entails estimating observables that may be contrasted with experimental data in order to offer a numerical evaluation of the theoretical frameworks covered in earlier chapters. Summary of the thesis are outlined in chapter 5. Additional information on the kinematics involved in the decay processes, as well as the system, is provided in the appendices A, B, C and D. Thorough analysis of the decay amplitude's relationship to partial decay rates is also included. These include particular frames of reference such as the hadron and lepton rest frame. It also covers more ground in the leptonic and hadronic portions of the decay, providing a fine-grained perspective on the distribution of final spin orientations, bilinears, and spinor representations. The form factors and Wilson coefficients, which are essential for the theoretical computations included in the thesis, are finally covered.

# Chapter 2

## Theoretical Framework

*This chapter discusses the primary notion of obtaining the Hamiltonian for decay and presents the theoretical background of it. We begin by talking about EFTs and flavor in the standard model. Next, we provide the idea of CKM matrices and explain why the GIM mechanism prevents FCNCs from happening at the tree level. We provide the operator product expansion that allows for the effective Hamiltonian to be derived.*

### 2.1 Effective Field Theory

Nature is full of mysteries, most interesting fact is occurrences of phenomenon over a broad range of energy, length, and time scales. However, particle physicists tend to think in terms of energy scales. EFTs are basic quantum field theory that is based on the principal of quantum mechanics, and special theory of relativity. In effective field theories experimentally determined quantities and their uncertainty are computed. The key component used in EFTs is locality, which allow us to separate the problem into different scales. This division help in the factorization of the field theory amplitudes into short-distance part named the wilson co-efficients and long-distance part which includes the matrix element. EFTs make it possible to efficiently arrange computations and estimate quantities by combining gauge invariance, locality, and the power counting formula [14].

#### 2.1.1 Why we use EFTs

Every theory we employ in physics today is really an EFT, whether we name it that or not. There are many reasons why we use EFT some of them are summarize as,

- The main purpose of using an EFT is that it simplifies our calculation and uses only the relevent interaction. For example, we are doing semileptonic b decay we do not need the full model with the higgs potential and everything else all we need is to care about the effective operator in the lagrangian and some constant term. We study these operator arises from W exchange between the quarks and not the full dynamic of the system.
- Another reason is that it separate out the scale i.e. the high and low energy scale which make the Feynman diagram easier to solve. For example in B meson decay there are various mass scale involved such as  $M_W$ ,  $m_b$  and  $\Lambda_{\text{QCD}}$ , and we can get very complicated functions of the ratios of these scales. But in EFT, we deals with one scale at a time, so there are no functions, only constants. Many theories are use for these purpose such as HQET, SCET, and NRQCD etc [14].

#### 2.1.2 Basic Ingredient of EFTs

Any EFT have main three ingredient which are discussed as follow,

- Degree of freedom: For any EFT the first building block is the degree of freedom that a physical system need to be describe in.
- Symmetries: Second block for building an EFT is symmetry. The symmetry for any dynamic system determined the constrain and limit of the effective action's and, thus, the system's dynamics. Symmetries in a system can appear in different ways: they can be global, gauged, accidental, spontaneously broken, anomalous, approximate, contracted, etc [15]. Looking at the symmetry we construct the lagrangian.
- Expansion Parameter: The key aspect in EFTs is the expansion parameter in which higher order correction term can be compute. Mostly but not always this expansion parameter is ratio between two scale. The low energy scale may be the momentum or mass of the particle to the short distance scale often denoted with  $\delta = \frac{p}{\Lambda}$ . In some theories such as HQET the expansion parameter may be perturbative a small coupling constant  $\alpha_s(m_b)$ .

### 2.1.3 General EFTs

Multi-scale problem are mostly discussed in EFT such as,

- **Standard model effective field theory (SMEFT)** main structure are field content, symmetries, and interactions. SMEFT are extended to higher dimension operator that are built on the same field and symmetries of the SM and not every operator are allowed. Furthermore, extra symmetry requirements that are not included in the fundamental symmetries of the SM can also be imposed at the SMEFT level. For example lepton and baryon number conservation or cancellation of neutral currents transition at the tree level. These are SM properties that result from unintentional symmetries. It work in the scale of  $\Lambda$  which is order of few TeV [16].
- **Fermi theory of weak interactions** is also a scale based theory for weak interactions of quarks. In this theory two mass scale are involve, first in order of mass of b-quark and other is mass of W-boson. The mass of the W-boson is very high compared to other scale so we integrate the heavy part. The power counting is  $\delta = \frac{p}{M_W}$ . This theory was developed earlier when the scale  $M_W$  and  $M_Z$  were not known.
- **Heavy quark effective theory (HQET)** describe limit of QCD where the heavy quarks mass  $m_Q$  goes to  $\infty$  as the four-velocity  $v^\mu$  is held fixed. This limit is suitable for physical systems in which light Dof interact with the heavy quark mass. The light degree of freedom usually carry four-momentum significantly less than the heavy quark mass. For example, a meson ( $Q\bar{q}$ ) where Q represent heavy quark and  $\bar{q}$  is light Dof. The nonperturbative scale of the strong interactions determines the size of such a meson as size  $\sim \frac{1}{\Lambda_{\text{QCD}}}$ . From uncertainty principle the momentum transfer to light Dof is  $p_1 \sim \Lambda_{\text{QCD}}$ . If the momentum transferred to  $m_Q$  is  $\delta p_1$ , change in  $\delta v^\mu = \frac{\delta p_1}{m_Q} \rightarrow 0$ . That's why in QCD the appropriate limit is taking the heavy quark mass four-velocity fixed and  $m_Q \rightarrow \infty$ . The mass of the heavy quark's in strong interactions become independent of its spin and mass. As a result, new spin-flavor symmetries emerge in this limit. In the nonperturbative realm, HQET is provided with predictive power by these approximate symmetries [17].
- **Non-relativistic quantum chromodynamics (NRQCD)** A nonrelativistic effective field theory for QCD is able to explain the dynamics of non-relativistic heavy quarks. An expression of this effective theory known as nonrelativistic QCD, or NRQCD [18]. Because NRQCD construction involves many scales, it has shown to be more complex than HQET construction. There are just two significant scales in HQET:  $\Lambda_{\text{QCD}}$  and  $m_Q$ . Two other significant scales in NRQCD are  $m v$  and  $m v^2$ , which represent the quarks' momentum and energy (where v is the normal quark velocity). In literature they are named as hard

$(m, m)$ , soft  $(m\nu, m\nu)$ , potential  $(m\nu^2, m\nu)$ , and ultrasoft  $(m\nu^2, m\nu^2)$ . All of these region must be accurately describe within effective field theory.

- **Chiral perturbation theory ( $\chi PT$ )** describes the low energy dynamics of global symmetry of strong interaction. It deal with the mesons and baryons. Chiral perturbation theory explains low momentum transfer of interactions of pions and nucleons. The expansion parameter is  $\frac{p}{\Lambda_\chi}$  where  $\Lambda_\chi$  is order of approximately 1GeV. This scale as known as chiral symmetry breaking [19].
- **Soft Collinear Effective Field Theory (SCET)** is also a QCD theory of highly energetic quark interacting with co-linear and soft gluons. It describe the energetic processes where the final state has small invariant mass compared to COM energy of collisions. As in HQET the decay of heavy hadron can be treated only when the four-momentum of the light Dof is small compared to  $m_Q$ . But when the light hadronic decay product had higher energy  $\mathcal{E} \sim m_Q$  then expansion in the power of  $\frac{1}{\mathcal{E}}$  should be performed. Therefore a large energy effective field theory should be constructed that explains the interaction between energetic quarks and soft gluons. Two low energy scales exist in SCET, which need to be appropriately taken into consideration when calculating power counting. It is easy to understand these scales when one studies the  $p$  of collinear quark. If the direction of the quark is along the light cone direction  $n^\nu$  with momentum  $Q \sim \mathcal{E} \sim m_Q$  then

$$p = (p^+, p^-, p^\perp) = Q(\lambda^2, 1, \lambda),$$

where  $\lambda$  is small parameter. Thus  $p^\perp \sim Q$  is the intermediate scale. So we count the power in term of  $\lambda$  rather than  $\frac{1}{m_Q}$ . In SCET the expansion parameter is  $\frac{\Lambda_{QCD}}{Q}$ ,  $\frac{M_J}{Q}$  and  $\frac{\alpha_s(Q)}{4\pi}$ , where  $Q$  is the COM energy of hard scattering process and  $M_J$  is mass of the jet [20].

## 2.2 Beyond Standard Model

In lack of any direct signal from LHC search for physics beyond standard model (BSM) effects can be conducted with Standard model effective theories (SMEFT) or higgs effective field theory (HEFT) [21]. The fact that BSM physics has not been directly discovered, if it does exist, it is far heavier than the EW scale and outside the reach of the LHC. It cannot describe process above a certain scale that as  $\Lambda \gg m_Z$  where  $m_Z$  is mass of Z-boson. Under this scale the SM give renormalizable term but above this there are higher power of energies in the denominator which give divergences. Hence BSM the lagrangian can be extended in higher power of  $\Lambda$  [22] as follow.

$$\mathcal{L}_{SM} = \mathcal{L}_{SM}^{(4)} + \frac{1}{\Lambda} \sum_n \mathcal{C}_n^{(5)} \mathcal{O}_n^{(5)} + \frac{1}{\Lambda^2} \sum_n \mathcal{C}_n^{(6)} \mathcal{O}_n^{(6)} + \mathcal{O}\left(\frac{1}{\Lambda^3}\right), \quad (2.1)$$

where  $\mathcal{L}_{SM}^{(4)}$  is the usual renormalize part of the standard model lagrangian contain two and four dimension operators. Where order five and six give BSM effect. The operator  $\mathcal{O}_n^{(i)}$  represent the n dimension operator and  $\mathcal{C}_n^{(i)}$  are dimensionless coupling constant known as Wilson co-efficient. Once the underlying high-energy theory is known we can integrate out the heavy fields, and the coefficients  $\mathcal{C}_n^{(i)}$  can be found. In literature there are different basis used for  $i = 6$  operator in the lagrangian. But as we know physics are irrelevant of the basis we used, there are some that suited well then the other. Thus  $b \rightarrow s$  are neutral current and flavor changing weak decays they are considered as sensitive probes where contribution of physics beyond the Standard Model can be indicated. [23].



## 2.3 Standard Model: As an EFT

To begin with SM as an EFT there are three basic ingredients in particular,

- Field content: First of all we need to specify the kind of fields that are present in our theory.
- The symmetries of the field must be satisfied: In addition to these fundamental symmetries SM can also have associated accidental symmetries.
- How these symmetries are realised and/or broken: For instance, in standard model the  $SU(2)_L \otimes U(1)_Y$  symmetry is spontaneously broken due to the structure of the Higgs sector, in particular of the Higgs potential.
- The renormalizability properties: finally, we need to specify whether or not the theory is UV-complete, that is, that can be extrapolated up to arbitrarily large energies being able to provide meaningful physical predictions.

## 2.4 Flavor in the Standard Model

Flavor sector of standard model is very important because of its high precise data. In flavor sector, besides the force carrier or mediator of interaction there contains twelve matter particles known as fermions. These fermions are categorized into two types: quarks and leptons. Leptons and quarks are further classified into three families or generation that appear as right-handed (singlet) or left-handed (doublet):

$$\begin{bmatrix} e^- & u \\ \nu_e & d \end{bmatrix}, \begin{bmatrix} \mu & s \\ \nu_\mu & c \end{bmatrix}, \begin{bmatrix} \tau & t \\ \nu_\tau & b \end{bmatrix}.$$

The standard model is a chiral theory so the left handed feild are  $SU(2)$  doublet are represented as follow.

$$\begin{pmatrix} l^- \\ \nu_l \end{pmatrix}_L, \begin{pmatrix} q_u \\ q_d \end{pmatrix}_L,$$

where the right handed partners transform as  $SU(2)$  singlet.

$$\begin{aligned} l_R^- &= e_R, \mu_R, \tau_R, \\ q_{uR} &= u_R, c_R, t_R, \\ q_{dR} &= d_R, s_R, b_R, \end{aligned}$$

there is no right-handed neutrino in the standard model picture.

Furthermore, each fermion particle is coupled to an antiparticle, and the quantum numbers of these antiparticles are the opposite of the fermion, meaning that the cosmos contains six antiquarks and six antileptons. The final component of the standard model is the higgs boson, through higgs mechanism which is process responsible for assigning masses to both gauge bosons and fermions. The interaction with the higgs-field leads to the acquisition of mass by elementary particles, necessitating the existence of a spin-0 higgs-boson. Due to its ability to couple with its own field, the Higgs-boson possesses a relatively substantial mass.

Flavor aspect of the standard model explain the classification of particle into bosons and fermions. Several field in standard model have same quantum number and they have same gauge representation so they are named as flavor in particle physics. Within the standard model the unbroken gauge group  $SU(3)_C \otimes U(1)_{EM}$  and the five representation of three generation of fermion are as follow [24].

1. Left-handed quark doublet  $Q_{Li}(3, 2)_{\frac{1}{6}}$ .
2. Right-handed Up type quark  $U_{Ri}(3, 1)_{\frac{2}{3}}$ .
3. Right-handed down-type quarks  $D_{Ri}(3, 1)_{-\frac{1}{3}}$ .
4. Left-handed leptons in the  $L_{Li}(1, 2)_{-\frac{1}{2}}$ .
5. Right-handed electron  $E_{Ri}(1, 1)_{-1}$ .

The interaction of fundamental particle is explained by two theme

1. The symmetry of Lagrangian and SSB pattern
2. The fermion and scalar representation.

The Lagrangian that is appropriate for gauge symmetry of (1) and particle content of standard consist of following three parts

$$\mathcal{L}_{SM} = \mathcal{L}_{Kinetic} + \mathcal{L}_{Higgs} + \mathcal{L}_{Yukawa}. \quad (2.2)$$

### $\mathcal{L}_{Kinetic}$

To maintain the gauge in-variance in kinetic term the simple derivative ( $\partial_\mu$ ) is replaced by covariant derivative ( $\mathcal{D}_\mu$ )

$$\mathcal{D}_\mu = \partial^\mu + \iota g_s \mathcal{G}_i^\mu L_i + \iota g \mathcal{W}_j^\mu T_j + \iota g' \mathcal{B}^\mu Y. \quad (2.3)$$

Here  $\mathcal{G}_i^\mu$  are the eight gluon fields where i runs from 1 to 8.  $L_i$  are  $SU(3)_C$  generators (the  $3 \times 3$  gell-mann matrices where  $L_i = \frac{1}{2}\lambda_i$ ).  $\mathcal{W}_j^\mu$  are the three weak interaction bosons feild,  $T_j$  are  $SU(2)_L$  generators (the  $2 \times 2$  pauli matrices where  $T_j = (\frac{1}{2})\tau_j$  for doublets, and 0 for singlets). And the final part  $B_\mu$  is the single hypercharge boson,  $Y$  are  $U(1)_Y$  charges. Kinetic terms define the propagation and interactions of gauge bosons such as photons, W and Z bosons, and gluons.

- U(1) for Electromagnetism (associated with the hypercharge  $Y$ ):

$$\mathcal{B}^{\mu\nu} = \partial^\mu \mathcal{B}^\nu - \partial^\nu \mathcal{B}^\mu$$

- SU(2) for Weak interactions:

$$\mathcal{W}^{\mu\nu} = \partial^\mu \mathcal{W}_j^\nu - \partial^\nu \mathcal{W}_j^\mu - g \epsilon_{ijk} \mathcal{W}_j^\mu \mathcal{W}_k^\nu$$

- SU(3) for Strong (QCD) interactions:

$$\mathcal{G}^{\mu\nu} = \partial^\mu \mathcal{G}_i^\nu - \partial^\nu \mathcal{G}_i^\mu - g_s f_{ijk} \mathcal{G}_j^\mu \mathcal{G}_k^\nu$$

These field strength tensors are squared and multiplied by a factor of -1/4 in the kinetic component in the entire Lagrangian for the standard model.  $\mathcal{L}_{Kinetic}$  is given by

$$\begin{aligned} \mathcal{L}_{Kinetic} = & -\frac{1}{4} \mathcal{G}_i^{\mu\nu} \mathcal{G}_{\mu\nu i} - \frac{1}{4} \mathcal{W}_j^{\mu\nu} \mathcal{W}_{\mu\nu j} - \frac{1}{4} \mathcal{B}_{\mu\nu} \mathcal{B}^{\mu\nu Q} - \iota \overline{Q_{Li}} \gamma^\mu \mathcal{D} Q_{Li} - \iota \overline{U_{Li}} \gamma^\mu \mathcal{D} U_{Li} \\ & - \iota \overline{D_{Ri}} \gamma^\mu \mathcal{D} D_{Ri} - \iota \overline{L_{Li}} \gamma^\mu \mathcal{D} L_{Li} - \iota \overline{E_{Li}} \gamma^\mu \mathcal{D} E_{Li}. \end{aligned} \quad (2.4)$$

This interaction Lagrangian is flavor universal and CP conserving. For five representation of three generation the kinetic Lagrangian have its own form for each quark and leptons. In standard model, the field strength tensors exist in the kinetic terms for the gauge fields. Each gauge group (U(1), SU(2), and SU(3)) is connected with its own field strength tensor.

### $\mathcal{L}_{Higgs}$

Dynamics of the higgs field is explained by this part of the lagrangian. The renowned Higgs boson, discovered in 2012, appears as a fluctuation of the Higgs field's constant value over space.  $\mathcal{L}_\phi$  represents not just how the Higgs field behaves on its own, but also how it interacts with itself [24].

The scalar self interaction Higgs potential is given by

$$\mathcal{L}_\phi = (\mathcal{D}^\mu \phi)(\mathcal{D}_\mu \phi) - \mu^2 \phi \phi - \lambda(\phi \phi)^2, \quad (2.5)$$

$$V_\phi = \mu^2 \phi \phi + \lambda(\phi \phi)^2. \quad (2.6)$$

The two parameter  $\lambda$  and  $\mu$  are Higgs mass and Vacuum expectation value respectively.

### $\mathcal{L}_{Yukawa}$

Fermions and the higgs field interaction are represented by the yukawa lagrangian. It's the portion that gives particles mass and is named after Hideki Yukawa!. When vacuum expectation value of the higgs field are zero, their interaction with other particles, give to them via the yukawa interactions. The degree of coupling between the higgs and other particle results in different masses.

The Yukawa part of the Lagrangian is divided into two parts, leptonic and quark sector. The quark Yukawa sector is

$$-\mathcal{L}_Y^{quark} = Y_{ij}^d \overline{Q_{Li}} \phi \mathcal{D}_{Rj} + Y_{ij}^u \overline{Q_{Li}} \tilde{\phi} U_{Rj} + h.c. \quad (2.7)$$

while lepton Yukawa interaction is given by

$$-\mathcal{L}_Y^{leptons} = Y_{ij}^e \overline{L_{Li}} \phi E_{Rj} + h.c. \quad (2.8)$$

where  $\tilde{\phi} = \iota \tau \phi^\dagger$  and  $Y^f$  are  $3 \times 3$  matrices with dimensionless coupling. These are describe in detailed in the next chapter.

Table 2.1: Properties of the Standard Model quarks and leptons.

Particle	m (GeV/c <sup>2</sup> )	Charge	Interactions
Leptons			
$e$	0.000511	-1	U(1) <sub>EM</sub>
$\nu_e$	$< 3 \times 10^{-9}$	0	SU(2) <sub>L</sub>
$\mu$	0.106	-1	U(1) <sub>EM</sub>
$\nu_\mu$	$< 1.9 \times 10^{-4}$	0	SU(2) <sub>L</sub>
$\tau$	$1.7770 \pm 0.00029$	-1	U(1) <sub>EM</sub>
$\nu_\tau$	$< 0.018$	0	SU(2) <sub>L</sub>
Quarks			
$u$	0.0015 to 0.003	+2/3	SU(3) <sub>C</sub> $\otimes$ SU(2) <sub>L</sub> $\otimes$ U(1) <sub>Y</sub>
$d$	0.003 to 0.007	-1/3	SU(3) <sub>C</sub> $\otimes$ SU(2) <sub>L</sub> $\otimes$ U(1) <sub>Y</sub>
$c$	$1.25 \pm 0.09$	+2/3	SU(3) <sub>C</sub> $\otimes$ SU(2) <sub>L</sub> $\otimes$ U(1) <sub>Y</sub>
$s$	$0.095 \pm 0.025$	-1/3	SU(3) <sub>C</sub> $\otimes$ SU(2) <sub>L</sub> $\otimes$ U(1) <sub>Y</sub>
$t$	$174.2 \pm 3.3$	+2/3	SU(3) <sub>C</sub> $\otimes$ SU(2) <sub>L</sub> $\otimes$ U(1) <sub>Y</sub>
$b$	$4.70 \pm 0.07$	-1/3	SU(3) <sub>C</sub> $\otimes$ SU(2) <sub>L</sub> $\otimes$ U(1) <sub>Y</sub>

The six flavor of quark are commonly divided into heavy (c, b, t) and light(u, d, s) quark as follow,

$$\begin{pmatrix} m_u = 0.005 \text{ GeV} \\ m_d = 0.009 \text{ GeV} \\ m_s = 0.175 \text{ GeV} \end{pmatrix} \ll 1 \text{ GeV} \leq \begin{pmatrix} m_c = (1.15 - 1.35) \text{ GeV} \\ m_b = (4.0 - 4.4) \text{ GeV} \\ m_t = 174 \text{ GeV} \end{pmatrix}. \quad (2.9)$$

## 2.5 Weak Interaction of Quarks

Flavor in the SM includes both quark and lepton. When quarks interacts via weak forces they changes flavor. This flavor changing processes does not occur via strong and electromagnetic forces. They are mainly of two type, namely

- Flavor changing charge current processes.
- Flavor changing neutral current processes.

### 2.5.1 Flavor Changing Neutral Current Transition

In particle physics, a phenomenon known as a flavor-changing neutral current (FCNCs) occurs when a fermion's flavor changes but its electric charge doesn't change. These processes are not allowed at tree level in standard model because they cannot be directly mediated by W-bosons. There is explanation why these processes should not occur as any two flavor changing process result in FCNC. Experimentally these processes are very rare and suppressed. For example the decay of  $K_L \rightarrow \mu^+ \mu^-$  that are neutral current transition is very rare compared to charge current  $K^+ \rightarrow \mu^+ \nu$  decay. For these processes to suppressed there must be some mechanism to describe its nature [25].

In SM these processes can happen through higher-order loop diagrams but not at the tree level. At first order they appear in triple vertices (penguin diagram) and quadratic vertices (box diagram). Example of penguin and box diagram are given in Figure 2.1 and 2.2. The higher order loop diagrams i.e, penguins are actually the first order contributions normally radiative corrections to the tree diagram. These processes are suppressed because they do not occur at tree level and second reason is the GIM mechanism.

- **Penguin Vertices:** They involve quark only have same charge but different flavor. They are calculated using elementary vertices and propagator. Penguin Diagram shown in Fig 2.1 below depicting a higher-order QCD process involving a loop with virtual top quarks (t) and W bosons, contributing to the flavor changing neutral current transitions between a bottom quark (b) and a strange quark (s).

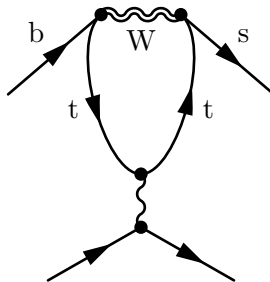


Figure 2.1: Penguin Diagram

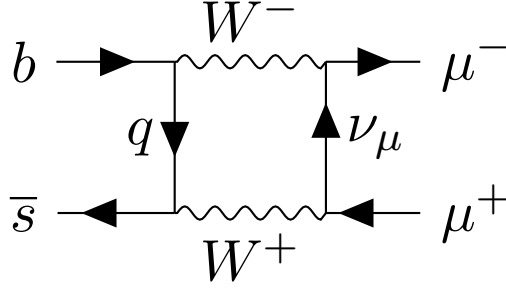


Figure 2.2: Box Diagram

- **Box Vertices:** They involve both quark and lepton calculated the same way as penguin diagram. A Feynman box diagram illustrates weak interaction process where a down quark (d) and a strange antiquark ( $\bar{s}$ ) exchange a W boson, resulting in the creation of a  $\mu^+$  and an  $\mu^-$ . The q and  $\nu_\mu$  are the internal line representing virtual particle.

### 2.5.2 The CKM Matrices

Unlike the gauge aspect of the SM, the flavor sector of the SM has not been verified to a high degree of precision. One of the most interesting problems in flavour physics is the determination of the CKM-matrix elements which dictate the degree of mixing between the quark weak and mass eigenstates in the weak interaction. The numerical results of these parameters are extracted from experimental data, prior to theoretical calculations.

The (CKM) matrix, referred as the Standard Model's Cabibbo-Kobayashi-Maskawa matrix, defines the mixing between the three generations of quarks. It explains why in weak interaction the weak eigenstates and their mass eigenstates are different [26]. The unitary cabibbo-kobayashi-maskawa (CKM) matrix is used to connect weak interactions basis to mass interaction basis of quarks.

By arranging the left-handed leptons with (chirality 1) in three generations of doublets and the right-handed leptons in three singlets states, the weak interaction for the leptons was added to the theory. Parallels between lepton and quark interactions suggest that organizing quarks into L-H doublets and R-H singlets is a comparable strategy for lepton interactions. For quarks, however, the situation is different since they all have mass. Consequently, a right-handed component is present in every quark field. Three doublets and six right-handed singlets make up these fields [27].

The kinetic terms and quark couplings to W, Z<sub>0</sub>, and  $\gamma$  are contained in the section of the lagrangian that is expressed as follows.

$$\mathcal{L} = \bar{q}_{Li} \gamma_\mu (i\partial^\mu + \frac{g}{2} W_b^\mu \tau_a - \frac{g'}{2} B^\mu Y) q_{Lj} + \bar{q}_{Ri} \gamma_\mu (i\partial^\mu - \frac{g'}{2} B^\mu Y) q_{Ri}. \quad (2.10)$$

The hypercharge Y is defined as  $Y = 2(Q - I_3)$ . Physical feild are eigenstate of mass matrix which are produced through quark-Higgs Yukawa coupling. It is simple to create a yukawa interaction term that is invariant under  $SU(2) \otimes U(1)$  transformations. The charge current interaction between the left handed quark is

$$\begin{aligned} \mathcal{L}_{\text{Kinetic, weak}}(Q_L) &= \overline{iQ_{Li}^I} \gamma_\mu (i\partial^\mu + \frac{g}{2} W_b^\mu \tau_a) Q_{Li}^I, \\ &= \overline{i(u, d)_{Li}^I} \gamma_\mu (i\partial^\mu + \frac{g}{2} W_b^\mu \tau_a) \begin{pmatrix} u \\ d \end{pmatrix}_{Li}^I, \end{aligned}$$

$$\begin{aligned}
&= \overline{\iota u_{Li}^I} \gamma_\mu \partial^\mu u_{Li}^I + \overline{\iota d_{Li}^I} \gamma_\mu \partial^\mu d_{Li}^I - \frac{g}{\sqrt{2}} \overline{\iota u_{Li}^I} \gamma_\mu W^{-\mu} d_{Li}^I - \frac{g}{\sqrt{2}} \overline{\iota d_{Li}^I} \gamma_\mu W^{+\mu} u_{Li}^I + \dots \\
\mathcal{L}_{mass} &= h_{(d)}^{ij} \begin{pmatrix} \bar{u}_i^1 \\ \bar{d}_i^1 \end{pmatrix}_L (\phi^+ \phi^0) d_{jR} + h_{(u)}^{ij} \begin{pmatrix} \bar{u}_i^1 \\ \bar{d}_i^1 \end{pmatrix}_L (-\bar{\phi}^0 \phi^-) u_{jR} + \text{h.c.} \quad (2.11)
\end{aligned}$$

using  $W^+ = \frac{1}{\sqrt{2}}(W_1 - \iota W_2)$  and  $W^- = \frac{1}{\sqrt{2}}(W_1 + \iota W_2)$ . The W boson acquire masses through the SSB. For this, the higgs scalar field and her potential is added to the Lagrangian:

$$\mathcal{L}_{\text{Higgs}} = (\mathcal{D}_\mu \phi)^\dagger (\mathcal{D}_\mu \phi) - \mu^2 \phi^\dagger \phi - \lambda (\phi^\dagger \phi)^2, \quad (2.12)$$

with iso-spin doublet that is

$$\phi = \begin{pmatrix} \phi^+ \\ \phi^0 \end{pmatrix}. \quad (2.13)$$

The Lagrangian is

$$\begin{aligned}
\mathcal{L}_{\text{mass}} &= Y_{ij} \bar{\Psi}_{Li} \phi \Psi_{Rj} + \text{h.c.} \\
&= Y_{ij}^d \bar{Q}_{Li}^I \phi d_{Rj}^i + Y_{ij}^u \bar{Q}_{Li}^I \tilde{\phi} u_{Rj}^i + Y_{ij}^l \bar{L}_{Li}^I \phi l_{Rj}^i + \text{h.c.} \quad (2.14)
\end{aligned}$$

we define  $Y_{ij}^{(u)}$ ,  $Y_{ij}^{(d)}$  and  $Y_{ij}^{(l)}$  are arbitrary complex matrices that operate in flavour space, giving rise to couplings between different families, or quark mixing, and thus to the field of flavour physics. These matrices are very important because these determined the masses of the quarks and also its mixing. In order to find the physical mass or mass eigenstate we need to transform the quark mass into diagonal form. Using bi-unitary transformation square matrix may be diagnosed [28]. Consequently, if we spell out one term

$$Y_{ij}^d \bar{Q}_{Li}^I \phi d_{Rj}^i = Y_{ij}^d \overline{(u \ d)_I^{Li}} \begin{pmatrix} \phi^+ \\ \phi^0 \end{pmatrix} d_{Rj}^i, \quad (2.15)$$

$$= \begin{pmatrix} Y_{11}^d \overline{(u \ d)_I^L} \begin{pmatrix} \phi^+ \\ \phi^0 \end{pmatrix} & Y_{12}^d \overline{(u \ d)_I^L} \begin{pmatrix} \phi^+ \\ \phi^0 \end{pmatrix} & Y_{13}^d \overline{(u \ d)_I^L} \begin{pmatrix} \phi^+ \\ \phi^0 \end{pmatrix} \\ Y_{21}^d \overline{(c \ s)_I^L} \begin{pmatrix} \phi^+ \\ \phi^0 \end{pmatrix} & Y_{22}^d \overline{(c \ s)_I^L} \begin{pmatrix} \phi^+ \\ \phi^0 \end{pmatrix} & Y_{23}^d \overline{(c \ s)_I^L} \begin{pmatrix} \phi^+ \\ \phi^0 \end{pmatrix} \\ Y_{31}^d \overline{(t \ b)_I^L} \begin{pmatrix} \phi^+ \\ \phi^0 \end{pmatrix} & Y_{32}^d \overline{(t \ b)_I^L} \begin{pmatrix} \phi^+ \\ \phi^0 \end{pmatrix} & Y_{33}^d \overline{(t \ b)_I^L} \begin{pmatrix} \phi^+ \\ \phi^0 \end{pmatrix} \end{pmatrix} \cdot \begin{pmatrix} d_R^I \\ s_R^I \\ b_R^I \end{pmatrix}. \quad (2.16)$$

After SSB

$$\phi = \begin{pmatrix} \phi^+ \\ \phi^0 \end{pmatrix} \xrightarrow{\text{breaking}} \phi = \frac{1}{\sqrt{2}} \begin{pmatrix} 0 \\ v + \eta \end{pmatrix}, \quad (2.17)$$

and charge conjugate of the Higgs field are obtained by taking complex conjugate and multiplying with Pauli matrices

$$\phi_c = -\iota \tau \phi^* \begin{pmatrix} -\bar{\phi}^0 \\ \phi^- \end{pmatrix} \xrightarrow{\text{breaking}} -\frac{1}{\sqrt{2}} \begin{pmatrix} v + \eta \\ 0 \end{pmatrix}, \quad (2.18)$$

$\eta$  is minimum value of feild fluctuation. The following mass term in fermion evolve in the lagrangian

$$= Y_{ij}^d \bar{Q}_{Li}^I \phi d_{Rj}^i + Y_{ij}^u \bar{Q}_{Li}^I \tilde{\phi} u_{Rj}^i + \text{h.c.},$$

$$\begin{aligned}
&= Y_{ij}^d \bar{d}_{Li}^I \frac{\nu}{\sqrt{2}} d_{Rj}^i + Y_{ij}^u \bar{u}_{Li}^I \frac{\nu}{\sqrt{2}} u_{Rj}^i + h.c., \\
&= M_{ij}^d \bar{d}_{Li}^I d_{Rj}^i + M_{ij}^u \bar{u}_{Li}^I u_{Rj}^i + h.c.
\end{aligned} \tag{2.19}$$

Fermionic interaction with the higgs feild are not considered here. The mass matrix should be diagonal so we need unitary matrix to diagonalize the mass matrix

$$\begin{aligned}
M_{diag}^d &= V_L^d M^d V_R^{d\dagger}, \\
M_{diag}^u &= V_L^u M^u V_R^{u\dagger},
\end{aligned} \tag{2.20}$$

as the unitary matrix satisfy  $V_R^d V_R^{d\dagger} = 1$ , the lagrangian can be written as

$$\begin{aligned}
&= \bar{d}_{Li}^I M_{ij}^d d_{Rj}^I + \bar{u}_{Li}^I M_{ij}^u u_{Rj}^I + h.c., \\
&= \bar{d}_{Li}^I V_L^d V_L^{d\dagger} M_{ij}^d V_R^d V_R^{d\dagger} d_{Rj}^I + \bar{u}_{Li}^I V_L^u V_L^{u\dagger} M_{ij}^u V_R^u V_R^{u\dagger} u_{Rj}^I + h.c., \\
&= \bar{d}_{Li}^I \left( M_{ij}^d \right)_{diag} d_{Rj}^I + \bar{u}_{Li}^I \left( M_{ij}^u \right)_{diag} u_{Rj}^I + h.c.
\end{aligned} \tag{2.21}$$

where quark states get the matrix, resulting in the following quark mass eigenstates,

$$\begin{aligned}
d_{Li} &= \left( V_L^d \right)_{ij} d_{Lj}^I d_{Ri} = \left( V_R^d \right)_{ij} d_{Rj}^I, \\
u_{Li} &= \left( V_L^u \right)_{ij} u_{Lj}^I u_{Ri} = \left( V_R^u \right)_{ij} d_{uj}^I,
\end{aligned} \tag{2.22}$$

where  $u^I$  are interaction eigen state and other are mass eigen state. We can also express the lagrangian in mass eigen state. The unitary  $3 \times 3$  is

$$V_{CKM} = \left( V_L^u V_L^{d\dagger} \right)_{ij}. \tag{2.23}$$

Conventionally, for up-type quarks, interaction/weak eigen state are equal to mass eigenstates because the matrix are absorbed inside the down type quarks. Whereas for down-type quarks are treated to be non equal.

$$\begin{aligned}
u_i^I &= u_j, \\
d_i^I &= V_{CKM} d_i,
\end{aligned} \tag{2.24}$$

or

$$\begin{pmatrix} d_I \\ s_I \\ b_I \end{pmatrix} = \begin{pmatrix} V_{ud} & V_{us} & V_{ub} \\ V_{cd} & V_{cs} & V_{cb} \\ V_{td} & V_{ts} & V_{tb} \end{pmatrix} \begin{pmatrix} d \\ s \\ b \end{pmatrix}, \tag{2.25}$$

where the transition from down to up quark is describe by  $V_{ud}$  while the transition from up to down quark is describe by  $V_{ud}^*$  shown in 2.3

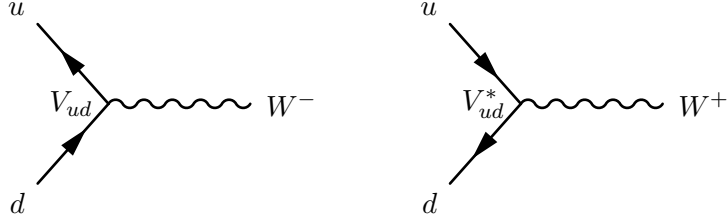


Figure 2.3: The definition of  $V_{ij}$  and  $V_{ij}^*$ .

### 2.5.3 GIM Mechanism

The Glashow-Iliopoulos-Maiani mechanism, developed in 1970 by Sheldon Glashow, Luciano Maiani, and John Iliopoulos, is referred to as the "GIM mechanism". This process is essential to the suppression of flavor-changing neutral currents (FCNCs) in particle physics standard model (SM) weak interactions. It also explains why the weak interaction that changes strangeness by  $S = 2$  are suppressed and why the transition  $S = 1$  are allowed only for charge currents (FCCCs) interaction. This mechanism to eliminates the strangeness changing neutral current at tree approximation is known as GIM mechanism. This mechanism was proposed by scientist before the discovery of strange quark.

The (GIM) method depends on the charged weak current flavor mixing matrix's unitarity. The magnitude of CKM parameters enters in the vertex where the  $W$ -boson and quark interacts. Although the  $Z^0$  bosons exchange are flavor neutral transition. In first order loop level decay the amplitude is proportional to  $m_i^2/M_w^2$  known as GIM mechanism [29]. The mass here is mass of internal quark.

## 2.6 Operator Product Expansion

$\Lambda$  is a hadron and the the quark inside are bind together via strong interaction. Weak decay of hadron are mediated by weak interaction of order of  $\mathcal{O}(1\text{GeV})$ . The goal is to achieve a precise theory to describe the weak interaction of quark. The task is tried to accomplished by using the operator product expansion.

OPE is QFT that describes the product of two field at each point in a limit  $x_n \rightarrow y$ . Thus, they capture the singular behavior and "finite trends" of products of quantum fields at a point [30]. As we know from  $\phi^4$  theory that the time ordered product of any two feild along with Fourier transformation can be written as

$$T\tilde{\phi}(p)\phi(0) = \int e^{ip \cdot x} T\tilde{\phi}(x)\phi(0) d^4x, \quad (2.26)$$

if the theory associated are totally defined then at  $x^\mu \rightarrow 0$  will give  $\phi^2(0)$ . But if it is not, then divergence appear from the products of feild. The OPE was given by Wilson in (1969). Its central idea was the product of the two local quantum feild operators can be written as

$$\mathcal{O}_{a1}(x_1)\dots\mathcal{O}_{aN}(x_N) \sim \sum_b \mathcal{C}_{a1\dots aN}^b(x_1\dots x_N)\mathcal{O}_b(x_N). \quad (2.27)$$

The product of two charge current operator can be written as expansion of local operator whose contribution are weighted by effective coupling constant, the wilson co-efficient. In 2.27  $\mathcal{C}_{a1\dots aN}^b(x_1\dots x_N)$  are the wilson co-efficient and  $\mathcal{O}_{aN}(x_N)$  are the local operators.



## 2.7 Effective Hamiltonian for FCNCs

The effective Hamiltonian for FCNCs processes in general may be expressed as follows from OPE [31]

$$\mathcal{H}_{eff} = \sum_k C_k(\mu) O_k(\mu), \quad (2.28)$$

where  $\mu$  is the appropriate re-normalization scale. The OPE allow us to divide the hamiltonian into long distance and short distance part. The former part is related to the non perturbative hadronic matrix element  $O_k(\mu) = \langle f | Q_k(\mu) | i \rangle$ , and  $C_k(\mu)$  are wilson coefficient calculated perturbatively. These wilson co-efficient are combination of some function and corresponding CKM matrix that can be read from the rule. The  $Q_k(\mu)$  are four quark operator that can be divided into three categories. The set of ten local operator is written as [32],

- Current Current Operator

$$\begin{aligned} Q_1 &= (\bar{s}_i u_j)_{V-A} (\bar{u}_j d_i)_{V-A}, \\ Q_2 &= (\bar{s} u)_{V-A} (\bar{u} d)_{V-A}. \end{aligned} \quad (2.29)$$

- QCD Penguin Operator

$$\begin{aligned} Q_3 &= (\bar{s} d)_{V-A} \sum_q (\bar{q} q)_{V-A}, \\ Q_4 &= (\bar{s}_i d_j)_{V-A} \sum_q (\bar{q}_j q_i)_{V-A}, \\ Q_5 &= (\bar{s} d)_{V-A} \sum_q (\bar{q} q)_{V+A}, \\ Q_6 &= (\bar{s}_i d_j)_{V-A} \sum_q (\bar{q}_j q_i)_{V+A}. \end{aligned} \quad (2.30)$$

- Electroweak-Penguins Operator

$$\begin{aligned} Q_7 &= \frac{3}{2} (\bar{s} d)_{V-A} \sum_q e_q (\bar{q} q)_{V+A}, \\ Q_8 &= \frac{3}{2} (\bar{s}_i d_j)_{V-A} \sum_q e_q (\bar{q}_j q_i)_{V+A}, \\ Q_9 &= \frac{3}{2} (\bar{s} d)_{V-A} \sum_q e_q (\bar{q} q)_{V-A}, \\ Q_{10} &= \frac{3}{2} (\bar{s}_i d_j)_{V-A} \sum_q e_q (\bar{q}_j q_i)_{V-A}. \end{aligned} \quad (2.31)$$

- Magnetic Penguin Operator

$$\begin{aligned} Q_{7\gamma} &= \frac{e}{8\pi^2} m_b (\bar{s} \sigma_{\mu\nu} (1 + \gamma_5) b) F_{\mu\nu}, \\ Q_{8G} &= \frac{e}{8\pi^2} m_b (\bar{s}_i \sigma_{\mu\nu} (1 + \gamma_5) T_{ij} b_j) G_{\mu\nu}. \end{aligned} \quad (2.32)$$

- Semi Leptonic Operator

$$\begin{aligned}
Q_{7V} &= (\bar{s}d)_{V-A}(\bar{e}e)_V, \\
Q_{9V} &= (\bar{b}s)_{V-A}(\bar{e}e)_V, \\
Q_{(\bar{\nu}\nu)} &= (\bar{s}d)_{V-A}(\bar{\nu}\nu)_{V-A}, \\
Q_{7A} &= (\bar{s}d)_{V-A}(\bar{e}e)_A, \\
Q_{10A} &= (\bar{b}s)_{V-A}(\bar{e}e)_A, \\
Q_{(\bar{\mu}\mu)} &= (\bar{s}d)_{V-A}(\bar{\mu}\mu)_{V-A}.
\end{aligned} \tag{2.33}$$

- $\Delta S = 2$  and  $\Delta B = 2$  Operators

$$\begin{aligned}
Q(\Delta S = 2) &= (\bar{s}d)_{V-A}(\bar{s}d)_{V-A}, \\
Q(\Delta B = 2) &= (\bar{b}d)_{V-A}(\bar{b}d)_{V-A}.
\end{aligned} \tag{2.34}$$

where  $V \pm A$  are chiral projection operator  $\gamma^\mu(1 \pm \gamma_5)$ ,  $\alpha$  and  $\beta$  are  $SU(3)_C$  color indices,  $q'$  runs over the quark flavors that are active at a scale of  $\mu = \mathcal{O}(m_b)$  i.e, u,d,s and c, and  $e'_q$  are the quark masses. These three operator who has maximum contribution in  $b \rightarrow s$  transition can be depicted in the penguin diagrams in 2.4.

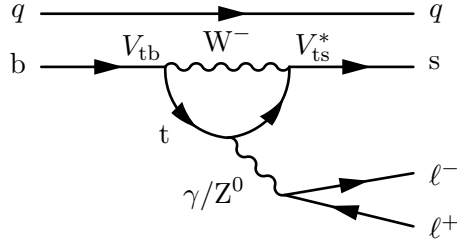


Figure 2.4: Penguin Diagram for FCNC  $b \rightarrow sl^+l^-$

# Chapter 3

## Formalism

We first go over the Effective Hamiltonian from the operator product expansion. We then turn to the hadronic coupling for quark level transitions  $b \rightarrow s$ . The helicity basis is used to calculate the hadronic matrix elements of  $b \rightarrow s$  and  $\Lambda \rightarrow N\pi$ . We next move on to observables and describe the approaches used for uncertainty calculation in our study. This chapter contains a detailed explanation of the formula we used to determine the branching ratio and other observables. The chapter concludes with a discussion of the possible consequences of new physics scenario effects that emerge from our findings.

### 3.1 Effective Hamiltonian

Effective hamiltonian for weak interaction of quarks is derived by calculating the leading and next-to-leading order loop diagrams. In the SM, effective hamiltonian is written using operator product expansion and re-normalization group techniques. The OPE that calculates the effective Hamiltonian describes the weak decays of hadrons. This hamiltonian can be divided into short distance perturbative physics and a long distance non-perturbative physics as discussed in the previous section. We have used the model independent approach, we do not restrict ourself to two type of current in lepton that are vector and axial vector. For semileptonic decay of  $\Lambda_b(u, d, b) \rightarrow \Lambda(u, d, s)l^+l^-$ , the effective within OPE can be written as:

$$\mathcal{H}_{eff} = \frac{4G_F\alpha}{\sqrt{2}}V_{tb}V_{ts}^* \left[ \sum_{i=1}^6 C_i \mathcal{Q}_i + \sum_{i=7}^8 (C_i \mathcal{Q}_i + C'_i \mathcal{Q}'_i) + \sum_{i=9,10} (C_i \mathcal{Q}_i + C_{il}^{NP} \mathcal{Q}_i + C_{i'l'}^{NP} \mathcal{Q}_{i'}) \right], \quad (3.1)$$

where  $\lambda_t = V_{ts}^\dagger V_{tb}$ , are CKM matrix element,  $G_f$  is the Fermi coupling constant,  $\mathcal{Q}_i(\mu)$  are local operators. These ten operators represent different types of physical processes, like current-current interactions, QCD penguin processes, magnetic penguin processes, and semileptonic electroweak penguin processes.  $C_i(\mu)$  are the wilson co-efficients that can be obtained from perturbative QCD and involves the short distance contribution. The long distance part are present in the matrix element of the local quark operators.

Decay of  $\Lambda_b \rightarrow \Lambda$  is basically a quark level transition from  $b \rightarrow s$  that are dominated by electroweak penguin process. Among these local operators the main contribution arises from  $\mathcal{O}_7$ ,  $\mathcal{O}_9$ , and  $\mathcal{O}_{10}$  in FCNCs decay channel. The main contributor are

$$\begin{aligned} \mathcal{O}_7 &= \frac{e}{8\pi^2} m_b (\bar{s}\sigma_{\mu\nu}(1 + \gamma_5)b)F_{\mu\nu}, \\ \mathcal{O}_9 &= \frac{e}{8\pi^2} (\bar{s}b)_{V-A}(\bar{l}l)_V, \\ \mathcal{O}_{10} &= \frac{e}{8\pi^2} (\bar{s}b)_{V-A}(\bar{l}l)_A. \end{aligned} \quad (3.2)$$

### 3.1.1 New physics in Effective Hamiltonian

These effect of physics beyond standard model in  $\Lambda_b$  decay can be interpreted in terms of different new physics (NP) scenarios with model in-dependant approach. Any high energy new physics will show up in whole new operators, in our case vector and axial vector part with chirality flipped counterpart that may be relevant for physics beyond standard model. Another way is incorporating new wilson-coefficient whose values are differ from those predicted in the SM. The co-efficient of higher dimension operator named as wilson co-efficient contain information about all short distance physics and NP are also incorporated here. The information about the numerical data of these co-efficient are taken from global fit analysis.

The primed operator correspond to right-handed current in the SM. The hypothesis that divides the  $C_{9,10}^{\text{NP}}$  and  $C_{9',10'}^{\text{NP}}$  are divided into Lepton flavor universality NP (LFU) and Lepton flavor violating universality NP (LFVU) are also used in the model independent analysis. All the short distance contribution are LFVU they are independent of the initial hadronic state and there kinematics.

The NP addition started at operator level and in this case the primed operator are NP operator. These operator that appear in these co-efficient are different given as,

$$\begin{aligned}\mathcal{O}'_7 &= \frac{e}{8\pi^2} m_b (\bar{s} \sigma_{\mu\nu} (1 - \gamma_5) b) F_{\mu\nu}, \\ \mathcal{O}'_9 &= \frac{e}{8\pi^2} (\bar{s} b)_{V+A} (\bar{l} l)_V, \\ \mathcal{O}'_{10} &= \frac{e}{8\pi^2} (\bar{s} b)_{V+A} (\bar{l} l)_A.\end{aligned}\tag{3.3}$$

The  $\mathcal{H}_{\text{eff}}$  can be written from equation 3.1 as

$$\begin{aligned}\mathcal{H}_{\text{eff}} &= \frac{4G_F\alpha}{\sqrt{2}} V_{tb} V_{ts}^* \left\{ \left( C_7^{\text{eff}} \frac{e}{8\pi^2} m_b \left( (\bar{s} \sigma_{\mu\nu} (1 + \gamma_5) b) F_{\mu\nu} \right) \right) \right. \\ &+ \left( C_9^{\text{eff}} \frac{e}{8\pi^2} (\bar{s} b)_{V-A} (\bar{l} l)_V + C_9^{\text{NP}} \frac{e}{8\pi^2} (\bar{s} b)_{V-A} (\bar{l} l)_V + C_{9'}^{\text{NP}} \frac{e}{8\pi^2} (\bar{s} b)_{V+A} (\bar{l} l)_V \right) \\ &\left. + \left( C_{10}^{\text{eff}} \frac{e}{8\pi^2} (\bar{s} b)_{V-A} (\bar{l} l)_A + C_{10}^{\text{NP}} \frac{e}{8\pi^2} (\bar{s} b)_{V-A} (\bar{l} l)_A + C_{10'}^{\text{NP}} \frac{e}{8\pi^2} (\bar{s} b)_{V+A} (\bar{l} l)_A \right) \right\}.\end{aligned}\tag{3.4}$$

## 3.2 Amplitude for $\Lambda_b \rightarrow \Lambda l^+ l^-$

The decay amplitude that contain hadronic matrix elements for  $\Lambda_b$  and  $\Lambda$  can be obtained by sand-witching the hamiltonian in 3.4 between the initial ( $\Lambda_b$ ) and final ( $\Lambda$ ) state. These matrix elements can be parameterized in terms of baryonic transition form factors for vector, axial-vector and tensor and pseudo-tensor currents [33]. The form factors are (i) defined in term of helicity basis and (ii) normalized to the limit of hadrons with point-like object. The decay amplitude for the quark level transition  $b \rightarrow s$  can be written in term of helicity basis using orthonormality and completeness relation of the polarization vector as follow. The completeness relation read as

$$\epsilon_\alpha^*(m) \epsilon^\beta(n) = g_{mn}, \quad \sum_{m,n=\pm,\mp,0} \epsilon_\alpha^*(m) \epsilon^\beta(n) g_{mn} = g^{\alpha\beta},\tag{3.5}$$

where complete description is given in Appendix B in equation B.3 .

Solving  $\mathcal{H}_{\text{eff}}$  the effective hamiltonian of 3.4 it takes the following form,

$$\mathcal{H}_{\text{eff}} = \frac{G_F\alpha}{2\sqrt{2}} V_{tb} V_{ts}^* \left\{ \left( (C_9^{\text{eff}} + C_9^{\text{NP}}) (\bar{s} b)_{V-A} (\bar{l} l)_V + C_{9'}^{\text{NP}} (\bar{s} b)_{V+A} (\bar{l} l)_V \right) \right\}$$

$$\begin{aligned}
& - \left( C_7^{eff} \frac{2m_b}{q^2} (\bar{s}l\sigma_{\mu\nu}(1+\gamma_5)q_\nu b)(\bar{l}l)_V \right) \\
& + \left( C_{10}^{eff} + C_{10}^{NP} \right) (\bar{s}b)_{V-A}(\bar{l}l)_A + C_{10'}^{NP} (\bar{s}b)_{V+A}(\bar{l}l)_A \Big\}.
\end{aligned}$$

Now taking vector and axial vector current common from above equation we get the following form

$$\begin{aligned}
\mathcal{H}_{\text{eff}} = \frac{G_f \alpha}{2\sqrt{2}} V_{tb} V_{ts}^* \Big\{ (\bar{l}l)_V \Big\{ \left( C_9^{eff} + C_9^{NP} \right) (\bar{s}b)_{V-A} + C_{9'}^{NP} (\bar{s}b)_{V+A} - C_7^{eff} \frac{2m_b}{q^2} (\bar{s}l\sigma_{\mu\nu}(1+\gamma_5)q_\nu b) \Big\} \\
(\bar{l}l)_A \Big\{ \left( C_{10}^{eff} + C_{10}^{NP} \right) (\bar{s}b)_{V-A} + C_{10'}^{NP} (\bar{s}b)_{V+A} \Big\}. \tag{3.6}
\end{aligned}$$

We have separated the leptonic part as vector and axial vector current, now we can write down the amplitude as

$$\mathcal{M}(b \rightarrow sl^+l^-) = \frac{G_f \alpha}{2\sqrt{2}} \left[ (\bar{l}\gamma^\mu l) A_\mu^1 + A_\mu^2 (\bar{l}\gamma^\mu \gamma^5 l) \right], \tag{3.7}$$

where  $\mathcal{A}_1^\mu$  and  $\mathcal{A}_2^\mu$  are defined explicitly as

$$\begin{aligned}
\mathcal{A}_1^\mu &= \left( C_9^{eff} + C_9^{NP} \right) \left[ \langle \Lambda(k, s_\Lambda) | \bar{s}\gamma^\mu (1 - \gamma^5) b | \Lambda_b(p, s_{\Lambda_b}) \rangle \right] \\
&+ C_{9'}^{NP} \left[ \langle \Lambda(k, s_\Lambda) | \bar{s}\gamma^\mu (1 + \gamma^5) b | \Lambda_b(p, s_{\Lambda_b}) \rangle \right] \\
&- \frac{2m_b}{q^2} C_7^{eff} \langle \Lambda(k, s_\Lambda) | \bar{s}l\sigma^{\mu\nu} q_\nu (1 + \gamma^5) b | \Lambda_b(p, s_{\Lambda_b}) \rangle. \\
\mathcal{A}_2^\mu &= \left( C_{10}^{eff} + C_{10}^{NP} \right) \left[ \langle \Lambda(k, s_\Lambda) | \bar{s}\gamma^\mu (1 - \gamma^5) b | \Lambda_b(p, s_{\Lambda_b}) \rangle \right] \\
&+ C_{10'}^{NP} \left[ \langle \Lambda(k, s_\Lambda) | \bar{s}\gamma^\mu (1 + \gamma^5) b | \Lambda_b(p, s_{\Lambda_b}) \rangle \right]. \tag{3.8}
\end{aligned}$$

the corresponding dagger of the amplitude is

$$\mathcal{M}^\dagger(b \rightarrow sl^+l^-) = \frac{G_f \alpha}{2\sqrt{2}} \left[ (\bar{l}\gamma^\nu l)^\dagger A_\nu^{1\dagger} + A_\nu^{2\dagger} (\bar{l}\gamma^\nu \gamma^5 l)^\dagger \right]. \tag{3.9}$$

The amplitude can be obtained by multiplying the dagger and non-dagger part of the Equation 3.7 and 3.9. We solve the leptonic traces and then contract it with the lepton polarization vector. Using the contraction of leptonic and hadronic tensor as shown

$$\begin{aligned}
\mathcal{L}_{\mu\nu}^1(m, n) &= p_{1\mu} p_{2\nu} \epsilon^{\mu\dagger}(m) \epsilon^\nu(n) + p_{2\nu} p_{1\mu} \epsilon^{\mu\dagger}(m) \epsilon^\nu(n) \\
\mathcal{L}_{\mu\nu}^2(m, n) &= \epsilon^{\mu\dagger}(m) \epsilon^\nu(n) g_{\mu\nu} \\
\mathcal{L}_{\mu\nu}^3(m, n) &= i \epsilon^{\mu\nu\alpha\beta} p_{1\alpha} p_{2\beta} \epsilon_{\mu\dagger}(m) \epsilon_\nu(n) \tag{3.10}
\end{aligned}$$

The hadronic part is given as,

$$\mathcal{H}_{ij}^{\mu\nu}(m, n) = \epsilon_\mu^\dagger(m) \epsilon_\nu(n) \mathcal{A}_{im}^\mu \bar{\mathcal{A}}_{jn}^\nu = \mathcal{H}_m^i(s_{\Lambda_b}, s_\Lambda) \mathcal{H}_n^{j\dagger}(s_{\Lambda_b}, s_\Lambda) \tag{3.11}$$

$m$  and  $n$  are the polarization vector element of the hadronic polarization vector in  $\Lambda_b$  rest frame.  $s_{\Lambda_b}$  and  $s_\Lambda$  are spin of the particle which are taken an account with angular momentum conservation. These hadronic term are the known as helicity amplitude because we solve the

matrix element in helicity basis. Using the properties of contraction of leptonic and hadronic tensor the amplitude formulae are modified as follow,

$$|\mathcal{M}|^2 = \frac{G_f^2 \alpha^2}{4.2} \left[ \mathcal{L}_{\mu\nu}^1 (\mathcal{H}_{11}^{\mu\nu} + \mathcal{H}_{22}^{\mu\nu}) - \frac{1}{2} \mathcal{L}_{\mu\nu}^2 (q^2 \mathcal{H}_{11}^{\mu\nu} + (q^2 - 4m_l^2) \mathcal{H}_{22}^{\mu\nu} + \mathcal{L}_{\mu\nu}^3 (\mathcal{H}_{12}^{\mu\nu} + \mathcal{H}_{21}^{\mu\nu})) \right], \quad (3.12)$$

where  $i, j = 1$  to  $3$ , and  $k = 1$  to  $2$  and they are described in detailed in the appendices.  $\mathcal{L}$  describe the leptonic part calculated from traces and  $\mathcal{H}_m^i(s_{\Lambda_b}, s_\Lambda) \mathcal{H}_n^{j\dagger}(s_{\Lambda_b}, s_\Lambda)$  are the helicity amplitude presented in detailed in appendices. The helicity amplitude are written in term of  $q^2$  dependant hadronic form factor.

### 3.2.1 Hadron Matrix Element Calculation

The form factors are (i) defined in term of helicity basis and (ii) normalized to the limit of hadrons with point-like object. All of the currents and their associated matrix element are given as follow

$$\begin{aligned} \langle \Lambda(k, s_\Lambda) | \bar{q} \gamma^\mu b | \Lambda_b(p, s_{\Lambda_b}) \rangle &= \bar{u}(k, s_\Lambda) [f_t(q^2) (M_{\Lambda_b} - m_\Lambda) \frac{q_\mu}{q^2} \\ &+ f_0(q^2) \frac{M_{\Lambda_b} + m_\Lambda}{s_+} (p_\mu + p'_\mu - \frac{q_\mu}{q^2} (M_{\Lambda_b}^2 - m_\Lambda^2)) \\ &+ f_\perp(q^2) (\gamma_\mu - \frac{2m_\Lambda}{s_+} p_\mu - \frac{2M_{\Lambda_b}}{s_+} p'_\mu)] u(p, s_{\Lambda_b}). \end{aligned}$$

The expression for axial current

$$\begin{aligned} \langle \Lambda(k, s_\Lambda) | \bar{q} \gamma_\mu \gamma_5 b | \Lambda_b(p, s_{\Lambda_b}) \rangle &= -\bar{u}(k, s_\Lambda) [g_t(q^2) (M_{\Lambda_b} + m_\Lambda) \frac{q_\mu}{q^2} \\ &+ g_0(q^2) \frac{M_{\Lambda_b} - m_\Lambda}{s_-} (p_\mu + p'_\mu - \frac{q_\mu}{q^2} (M_{\Lambda_b}^2 - m_\Lambda^2)) \\ &+ g_\perp(q^2) (\gamma_\mu + \frac{2m_\Lambda}{s_-} p_\mu - \frac{2M_{\Lambda_b}}{s_-} p'_\mu)] u(p, s_{\Lambda_b}). \end{aligned}$$

The expression for tensor current

$$\begin{aligned} \langle \Lambda(k, s_\Lambda) | \bar{q} \iota \sigma_{\mu\nu} q^\nu s | \Lambda_b(p, s_{\Lambda_b}) \rangle &= -\bar{u}(k, s_\Lambda) [h_0(q^2) \frac{q^2}{s_+} (p_\mu + p'_\mu - \frac{q_\mu}{q^2} (M_{\Lambda_b}^2 - m_\Lambda^2)) \\ &+ h_\perp(q^2) (M_{\Lambda_b} + m_\Lambda) (\gamma_\mu - \frac{2m_\Lambda}{s_+} p_\mu - \frac{2M_{\Lambda_b}}{s_+} p'_\mu)] u(p, s_{\Lambda_b}). \end{aligned}$$

The expression for pseudo-tensor current

$$\begin{aligned} \langle \Lambda(k, s_\Lambda) | \bar{q} \iota \sigma_{\mu\nu} \gamma_5 q^\nu s | \Lambda_b(p, s_{\Lambda_b}) \rangle &= -\bar{u}(k, s_\Lambda) [h_0(q^2) \frac{q^2}{s_-} (p_\mu + p'_\mu - \frac{q_\mu}{q^2} (M_{\Lambda_b}^2 - m_\Lambda^2)) \\ &+ h_\perp(M_{\Lambda_b} - m_\Lambda) (q^2) (\gamma_\mu + \frac{2m_\Lambda}{s_-} p_\mu - \frac{2M_{\Lambda_b}}{s_-} p'_\mu)] u(p, s_{\Lambda_b}). \end{aligned}$$

These form factor considerably reduce to much simpler form when contracted with polarization vector of hadronic spinor. These vector currents give three independent helicity form factors

that we named as the corresponding helicity amplitude  $H_i^{currents}(s_{\Lambda_b}, s_{\Lambda})$ . For vector current,

$$\begin{aligned} H_V^t(s_{\Lambda_b}, s_{\Lambda}) &\equiv \epsilon_{\mu}^*(t) \langle \Lambda(k, s_{\Lambda}) | \bar{s} \gamma^{\mu} b | \Lambda_b(p, s_{\Lambda_b}) \rangle \\ &= f_V^t(q^2) \frac{m_{\Lambda_b} - m_{\Lambda}}{\sqrt{q^2}} \bar{u}(k, s_{\Lambda}) u(p, s_{\Lambda_b}), \end{aligned}$$

$$\begin{aligned} H_V^0(s_{\Lambda_b}, s_{\Lambda}) &\equiv \epsilon_{\mu}^*(0) \langle \Lambda(k, s_{\Lambda}) | \bar{s} \gamma^{\mu} b | \Lambda_b(p, s_{\Lambda_b}) \rangle \\ &= 2f_V^0(q^2) \frac{m_{\Lambda_b} + m_{\Lambda}}{s_+} (k \cdot \epsilon^*(0)) \bar{u}(k, s_{\Lambda}) u(p, s_{\Lambda_b}), \end{aligned}$$

$$\begin{aligned} H_V^{\pm}(s_{\Lambda_b}, s_{\Lambda}) &\equiv \epsilon_{\mu}^*(\pm) \langle \Lambda(k, s_{\Lambda}) | \bar{s} \gamma^{\mu} b | \Lambda_b(p, s_{\Lambda_b}) \rangle \\ &= f_V^{\pm}(q^2) \bar{u}(k, s_{\Lambda}) \epsilon^*(\pm) u(p, s_{\Lambda_b}). \end{aligned}$$

Analogous expressions are obtained for the axial-vector current,

$$\begin{aligned} H_{AV}^t(s_{\Lambda_b}, s_{\Lambda}) &\equiv \epsilon_{\mu}^*(t) \langle \Lambda(k, s_{\Lambda}) | \bar{s} \gamma^{\mu} b | \Lambda_b(p, s_{\Lambda_b}) \rangle \\ &= -f_{AV}^t(q^2) \frac{m_{\Lambda_b} + m_{\Lambda}}{\sqrt{q^2}} \bar{u}(k, s_{\Lambda}) u(p, s_{\Lambda_b}), \end{aligned}$$

$$\begin{aligned} H_{AV}^0(s_{\Lambda_b}, s_{\Lambda}) &\equiv \epsilon_{\mu}^*(0) \langle \Lambda(k, s_{\Lambda}) | \bar{s} \gamma^{\mu} b | \Lambda_b(p, s_{\Lambda_b}) \rangle \\ &= -2f_{AV}^0(q^2) \frac{m_{\Lambda_b} - m_{\Lambda}}{s_-} (k \cdot \epsilon^*(0)) \bar{u}(k, s_{\Lambda}) u(p, s_{\Lambda_b}), \end{aligned}$$

$$\begin{aligned} H_{AV}^{\pm}(s_{\Lambda_b}, s_{\Lambda}) &\equiv \epsilon_{\mu}^*(\pm) \langle \Lambda(k, s_{\Lambda}) | \bar{s} \gamma^{\mu} b | \Lambda_b(p, s_{\Lambda_b}) \rangle \\ &= f_{AV}^{\pm}(q^2) \bar{u}(k, s_{\Lambda}) \epsilon^*(\pm) \gamma_5 u(p, s_{\Lambda_b}). \end{aligned}$$

Tensor current

$$\begin{aligned} H_T^0(s_{\Lambda_b}, s_{\Lambda}) &\equiv \epsilon_{\mu}^*(0) \langle \Lambda(k, s_{\Lambda}) | \bar{s}_i \sigma_{\nu}^{\mu} q^{\nu} b | \Lambda_b(p, s_{\Lambda_b}) \rangle \\ &= -2f_T^0(q^2) \frac{q^2}{s_+ (k \cdot \epsilon^*(0))} \bar{u}(k, s_{\Lambda}) u(p, s_{\Lambda_b}), \\ H_T^{\pm}(s_{\Lambda_b}, s_{\Lambda}) &\equiv \epsilon_{\mu}^*(\pm) \langle \Lambda(k, s_{\Lambda}) | \bar{s}_i \sigma_{\nu}^{\mu} q^{\nu} b | \Lambda_b(p, s_{\Lambda_b}) \rangle \\ &= -f_T^{\pm}(q^2) (m_{\Lambda_b} + m_{\Lambda}) \bar{u}(k, s_{\Lambda}) \epsilon^*(\pm) u(p, s_{\Lambda_b}). \end{aligned}$$

PseudoTensor currents

$$\begin{aligned} H_{T5}^0(s_{\Lambda_b}, s_{\Lambda}) &\equiv \epsilon_{\mu}^*(0) \langle \Lambda(k, s_{\Lambda}) | \bar{s}_i \sigma_{\nu}^{\mu} q^{\nu} \gamma^5 b | \Lambda_b(p, s_{\Lambda_b}) \rangle \\ &= -2f_{T5}^0(q^2) \frac{q^2}{s_- (k \cdot \epsilon^*(0))} \bar{u}(k, s_{\Lambda}) \gamma^5 u(p, s_{\Lambda_b}), \\ H_{T5}^{\pm}(s_{\Lambda_b}, s_{\Lambda}) &\equiv \epsilon_{\mu}^*(\pm) \langle \Lambda(k, s_{\Lambda}) | \bar{s}_i \sigma_{\nu}^{\mu} q^{\nu} \gamma^5 b | \Lambda_b(p, s_{\Lambda_b}) \rangle \\ &= f_{T5}^{\pm}(q^2) (m_{\Lambda_b} - m_{\Lambda}) \bar{u}(k, s_{\Lambda}) \epsilon^*(\pm) \gamma^5 u(p, s_{\Lambda_b}). \end{aligned}$$

## Non-zero Helicity Amplitude

Appendix C provides a summary of the hadronic spinor matrix elements for specific spin orientation combinations. Non-zero helicity amplitudes in the case of vector current, we obtain [11].

$$-\mathcal{H}_V^t(+\frac{1}{2}, -\frac{1}{2}) = \mathcal{H}_V^t(-\frac{1}{2}, +\frac{1}{2}) = f_V^t(q^2) \frac{(m_{\Lambda_b} - m_\Lambda)}{\sqrt{q^2}} \sqrt{s_+},$$

$$-\mathcal{H}_V^0(+\frac{1}{2}, -\frac{1}{2}) = \mathcal{H}_V^0(-\frac{1}{2}, +\frac{1}{2}) = f_V^t(q^2) \frac{(m_{\Lambda_b} + m_\Lambda)}{\sqrt{q^2}} \sqrt{s_-},$$

$$\mathcal{H}_V^+(\frac{1}{2}, +\frac{1}{2}) = \mathcal{H}_V^-(\frac{1}{2}, -\frac{1}{2}) = -f_V^\perp(q^2) \sqrt{s_-}.$$

Axial vector current non zero helicity amplitude

$$\mathcal{H}_{AV}^t(+\frac{1}{2}, -\frac{1}{2}) = -\mathcal{H}_{AV}^t(-\frac{1}{2}, +\frac{1}{2}) = f_{AV}^t(q^2) \frac{(m_{\Lambda_b} + m_\Lambda)}{\sqrt{q^2}} \sqrt{s_-},$$

$$\mathcal{H}_{AV}^0(+\frac{1}{2}, -\frac{1}{2}) = -\mathcal{H}_{AV}^0(-\frac{1}{2}, +\frac{1}{2}) = f_{AV}^t(q^2) \frac{(m_{\Lambda_b} - m_\Lambda)}{\sqrt{q^2}} \sqrt{s_+},$$

$$\mathcal{H}_{AV}^+(\frac{1}{2}, +\frac{1}{2}) = \mathcal{H}_{AV}^-(\frac{1}{2}, -\frac{1}{2}) = -f_{AV}^\perp(q^2) \sqrt{s_+}.$$

Tensor current non zero helicity amplitude,

$$-\mathcal{H}_T^0(+\frac{1}{2}, -\frac{1}{2}) = \mathcal{H}_T^0(-\frac{1}{2}, +\frac{1}{2}) = f_T^0(q^2) \sqrt{q^2} \sqrt{s_-},$$

$$\mathcal{H}_T^+(\frac{1}{2}, +\frac{1}{2}) = -\mathcal{H}_T^-(\frac{1}{2}, -\frac{1}{2}) = f_T^\perp(q^2) (m_{\Lambda_b} + m_\Lambda) \sqrt{2s_+}.$$

Pseudo-Tensor current non zero helicity amplitude,

$$\mathcal{H}_{T5}^0(+\frac{1}{2}, -\frac{1}{2}) = \mathcal{H}_{T5}^0(-\frac{1}{2}, +\frac{1}{2}) = -f_{T5}^0(q^2) \sqrt{q^2} \sqrt{s_+},$$

$$\mathcal{H}_{T5}^+(\frac{1}{2}, +\frac{1}{2}) = \mathcal{H}_{T5}^-(\frac{1}{2}, -\frac{1}{2}) = -f_{T5}^\perp(q^2) (m_{\Lambda_b} - m_\Lambda) \sqrt{2s_+}.$$

These are the helicity amplitude for  $\Lambda \rightarrow \Lambda l^+ l^-$ . The ten  $q^2$  dependent helicity form factor that are used in  $\Lambda_b \rightarrow \Lambda$  hadronic matrix element are discussed in appendix C in detailed. We use the form factors from the lattice QCD computation in numerical analysis [4], [5]. The lattice computations are restricted to two z-parameterizations in order to derive the  $q^2$  dependency and estimate the uncertainties. They are so called nominal fitting and higher order fitting. In the matrix element these information are buried in form factors. The explicit formulae for the form factor are written in appendix C [5].



## Helicity Amplitude for $\Lambda_b \rightarrow \Lambda l^+ l^-$

We write down the form factor of hadronic-matrix-element in helicity basis. We then introduced the spin matrix element and presented all the possible term. For our amplitude we defined the helicity amplitude in 3.11, we give all the non zero term that involve the standard model and new physics wilson co-efficient.

$$\begin{aligned}
\mathcal{H}_\pm^2(\pm\frac{1}{2}, \pm\frac{1}{2}) &= \pm\sqrt{2s_-} \left[ (C_{10}^{\text{eff}} + C_{10}^{\text{NP}} + C_{10'}^{\text{NP}}) f_\perp^V \right], \\
&\quad - \sqrt{2s_+} \left[ (C_{10}^{\text{eff}} + C_{10}^{\text{NP}} - C_{10'}^{\text{NP}}) f_\perp^A \right], \\
\mathcal{H}_t^1(\pm\frac{1}{2}, \mp\frac{1}{2}) &= \mp \frac{m_{\Lambda_b} - m_\Lambda}{\sqrt{q^2}} \sqrt{s_+} (C_9^{\text{eff}} + C_9^{\text{NP}} + C_{9'}^{\text{NP}}) f_t^V, \\
&\quad - \frac{m_{\Lambda_b} + m_\Lambda}{\sqrt{q^2}} \sqrt{s_-} (C_9^{\text{eff}} + C_9^{\text{NP}} - C_{9'}^{\text{NP}}) f_t^{AV}, \\
\mathcal{H}_t^2(\pm\frac{1}{2}, \mp\frac{1}{2}) &= \mp \frac{m_{\Lambda_b} - m_\Lambda}{\sqrt{q^2}} \sqrt{s_+} (C_{10}^{\text{eff}} + C_{10}^{\text{NP}} + C_{10'}^{\text{NP}}) f_t^V, \\
&\quad - \frac{m_{\Lambda_b} + m_\Lambda}{\sqrt{q^2}} \sqrt{s_-} (C_{10}^{\text{eff}} + C_{10}^{\text{NP}} - C_{10'}^{\text{NP}}) f_t^{AV}, \\
\mathcal{H}_0^2(\pm\frac{1}{2}, \mp\frac{1}{2}) &= \mp \frac{\sqrt{s_-}}{\sqrt{q^2}} (C_{10}^{\text{eff}} + C_{10}^{\text{NP}} + C_{10'}^{\text{NP}}) (m_{\Lambda_b} + m_\Lambda) f_0^V, \\
&\quad - \frac{\sqrt{s_+}}{\sqrt{q^2}} (C_{10}^{\text{eff}} + C_{10}^{\text{NP}} - C_{10'}^{\text{NP}}) (m_{\Lambda_b} - m_\Lambda) f_0^A, \\
\mathcal{H}_0^1(\pm\frac{1}{2}, \mp\frac{1}{2}) &= \mp \frac{\sqrt{s_-}}{\sqrt{q^2}} (C_9^{\text{eff}} + C_9^{\text{NP}} + C_{9'}^{\text{NP}}) (m_{\Lambda_b} + m_\Lambda) f_0^V + 2m_b C_7^{\text{eff}} f_0^T, \\
&\quad - \frac{\sqrt{s_+}}{\sqrt{q^2}} (C_9^{\text{eff}} + C_9^{\text{NP}} - C_{9'}^{\text{NP}}) (m_{\Lambda_b} - m_\Lambda) f_0^A + 2m_b C_7^{\text{eff}} f_0^{T5}, \\
\mathcal{H}_\pm^1(\pm\frac{1}{2}, \pm\frac{1}{2}) &= \pm\sqrt{2s_-} \left[ (C_9^{\text{eff}} + C_9^{\text{NP}} + C_{9'}^{\text{NP}}) f_\perp^V + \frac{2m_b}{q^2} C_7^{\text{eff}} (m_{\Lambda_b} + m_\Lambda) f_\perp^T \right], \\
&\quad - \sqrt{2s_+} \left[ (C_9^{\text{eff}} + C_9^{\text{NP}} - C_{9'}^{\text{NP}}) f_\perp^A + \frac{2m_b}{q^2} C_7^{\text{eff}} (m_{\Lambda_b} - m_\Lambda) f_\perp^{T5} \right]. \tag{3.13}
\end{aligned}$$

We uses these helicity amplitude in the final four fold decay width in section 3.3.

### 3.2.2 Hadronic Coupling for $\Lambda(u, d, s) \rightarrow N\pi$

In SM, the effective hamiltonian for the  $\Lambda \rightarrow N\pi$  is

$$\mathcal{H}^{eff} = \frac{4G_f}{\sqrt{2}} V_{ud}^* V_{us} [\bar{d}\gamma_\mu(1 - \gamma_5)u][\bar{u}\gamma_\mu(1 - \gamma_5)s]. \tag{3.14}$$

The parameterization of the hadronic-matrix-element governing the  $\Lambda\pi$  decay can be expressed as follows:

$$\begin{aligned}
&\langle p(k_1, s_N)\pi^-(k_2) | \bar{d}\gamma^\mu P_L u | \bar{u}\gamma^\mu P_L s \rangle \Lambda(k, s_\Lambda) \\
&= \langle \bar{u}(k_1, s_N) | \xi\gamma^5 + \omega u(k, s_\Lambda) \rangle \equiv H_2(s_\Lambda, s_N).
\end{aligned}$$

### Helicity Amplitude for $\Lambda(\mathbf{u}, \mathbf{d}, \mathbf{s}) \rightarrow N\pi$

The non-zero helicity-amplitude for  $\Lambda(u, d, s) \rightarrow N\pi$  decay can be deduced from the following formulae,

$$\Gamma_2(s_\Lambda^a, s_\Lambda^b) = \sum_{s_N} H_2(s_\Lambda^a, s_N) H_2^*(s_\Lambda^b, s_N), \quad (3.15)$$

which yields,

$$\begin{aligned} \Gamma_2(+, +) &= (1 + \alpha \cos \theta_\Lambda) \frac{\Gamma_\Lambda}{2}, \\ \Gamma_2(-, -) &= (1 - \alpha \cos \theta_\Lambda) \frac{\Gamma_\Lambda}{2}, \\ \Gamma_2(+, -) &= -\alpha \sin \theta_\Lambda \frac{\Gamma_\Lambda}{2}, \\ \Gamma_2(-, +) &= -\alpha \sin \theta_\Lambda \frac{\Gamma_\Lambda}{2}. \end{aligned} \quad (3.16)$$

where  $\Gamma_\Lambda$  contain information about phase space of  $N\pi$  system that approximately give one after putting the numerical value [2].

### 3.3 Four fold differential distribution in the cascade decay

For the given decay, we obtained the helicity amplitude in two steps. We first determine the decay rates as discussed in appendix A in order to derive the four fold differential decay distribution and related measurements like the branching ratio, etc. By multiplying the decay's amplitudes while taking the conservation of baryon momentum into consideration, the final four-fold distribution is achieved. By combining the decay amplitude of  $\Lambda_b \rightarrow \Lambda l^+ l^-$  and  $\Lambda \rightarrow N\pi$ , we get proceed with the general formulae for our ease,

$$\mathcal{M}_{\mathcal{F}\mathcal{F}} = \sum_{s_N} H_2(s_\Lambda^a, s_N) H_2^*(s_\Lambda^b, s_N) \sum_{s_{\Lambda_b}, s_\Lambda} H_m^i(s_{\Lambda_b}, s_\Lambda) \bar{H}_n^j(s_{\Lambda_b}, s_\Lambda). \quad (3.17)$$

In quantum mechanics, the squared transition matrix components are multiplied by phase space to get the distributions of angular decay. Phase space for a two-body decay is multiplied by matrix elements to determine the angular decay distribution for straightforward two-body decays i.e,  $\Lambda_b \rightarrow \Lambda l^+ l^-$ . The matrix elements are multiplied according to equation 3.17 whereas the phase space is simply multiplied for our four fold differential decay rate. Formulae for differential decay rate for our two system are given as,

$$\begin{aligned} \frac{d^2\Gamma}{dq^2 d \cos \theta_l} &= \frac{G_F^2}{(2\pi)^3} \left( \frac{\alpha \lambda_t}{2\pi} \right)^2 \frac{|k|\nu}{8m_{\Lambda_b}^2} \\ &\left[ L_{\mu\nu}^1 (\mathcal{H}_{11}^{\mu\nu} + \mathcal{H}_{22}^{\mu\nu}) - \frac{1}{2} L_{\mu\nu}^2 (q^2 \mathcal{H}_{11}^{\mu\nu} + (q^2 - 4m_l^2) \mathcal{H}_{22}^{\mu\nu} + L_{\mu\nu}^3 (\mathcal{H}_{12}^{\mu\nu} + \mathcal{H}_{21}^{\mu\nu})) \right]. \end{aligned} \quad (3.18)$$

The final four-fold differential decay rate of  $\Lambda_b \rightarrow \Lambda(\rightarrow N\pi) l^+ l^-$  is obtained by multiplying the amplitude of both part of our decay. The multiplication is taken in accordance with the kinematics of the state taken into account and also the spin of hadron that are  $\Lambda_b$ ,  $\Lambda$  and  $N$ .

$$\frac{d^4\Gamma}{dq^2 d \cos \theta_l d \cos \theta_\Lambda d\phi} = \frac{G_F^2}{(2\pi)^3} \left( \frac{\alpha \lambda_t}{2\pi} \right)^2 \frac{|k|\nu}{8m_{\Lambda_b}^2}$$

$$\begin{aligned}
& L_{\mu\nu}^1 \left[ \sum_{s_N} H_2(s_\Lambda^a, s_N) H_2^*(s_\Lambda^b, s_N) \left( \sum_{s_{\Lambda_b}, s_\Lambda} H_m^1(s_{\Lambda_b}, s_\Lambda) \bar{H}_n^{1*}(s_{\Lambda_b}, s_\Lambda) + \sum_{s_{\Lambda_b}, s_\Lambda} H_m^2(s_{\Lambda_b}, s_\Lambda) \bar{H}_n^{2*}(s_{\Lambda_b}, s_\Lambda) \right) \right] \\
& - \frac{1}{2} L_{\mu\nu}^2 \cdot q^2 \left( \sum_{s_N} H_2(s_\Lambda^a, s_N) H_2^*(s_\Lambda^b, s_N) \sum_{s_{\Lambda_b}, s_\Lambda} H_m^1(s_{\Lambda_b}, s_\Lambda) \bar{H}_n^{1*}(s_{\Lambda_b}, s_\Lambda) \right) \\
& + (q^2 - 4m_l^2) \cdot L_{\mu\nu}^2 \cdot \left( \sum_{s_N} H_2(s_\Lambda^a, s_N) H_2^*(s_\Lambda^b, s_N) \sum_{s_{\Lambda_b}, s_\Lambda} H_m^2(s_{\Lambda_b}, s_\Lambda) \bar{H}_n^{2*}(s_{\Lambda_b}, s_\Lambda) \right) \\
& + L_{\mu\nu}^3 \left( \sum_{s_N} H_2(s_\Lambda^a, s_N) H_2^*(s_\Lambda^b, s_N) \sum_{s_{\Lambda_b}, s_\Lambda} H_m^1(s_{\Lambda_b}, s_\Lambda) \bar{H}_n^{2*}(s_{\Lambda_b}, s_\Lambda) \right) \\
& + L_{\mu\nu}^3 \left( \sum_{s_N} H_2(s_\Lambda^a, s_N) H_2^*(s_\Lambda^b, s_N) \sum_{s_{\Lambda_b}, s_\Lambda} H_m^2(s_{\Lambda_b}, s_\Lambda) \bar{H}_n^{1*}(s_{\Lambda_b}, s_\Lambda) \right). \quad (3.19)
\end{aligned}$$

We write down the  $\Lambda \rightarrow N\pi$  spin orientation that modify the equation as follow,

$$\begin{aligned}
& \frac{d^4\Gamma}{dq^2 d \cos \theta_l d \cos \theta_\Lambda d\phi} = \frac{G_F^2}{(2\pi)^3} \left( \frac{\alpha\lambda_t}{2\pi} \right)^2 \frac{|k|\nu}{8m_{\Lambda_b}^2} \\
& L_{\mu\nu}^1 \left[ \Gamma_2(s_\Lambda^a, s_\Lambda^b) \left( \sum_{s_{\Lambda_b}, s_\Lambda} H_m^1(s_{\Lambda_b}, s_\Lambda) \bar{H}_n^{1*}(s_{\Lambda_b}, s_\Lambda) + \sum_{s_{\Lambda_b}, s_\Lambda} H_m^2(s_{\Lambda_b}, s_\Lambda) \bar{H}_n^{2*}(s_{\Lambda_b}, s_\Lambda) \right) \right] \\
& - \frac{1}{2} L_{\mu\nu}^2 \cdot q^2 \left( \Gamma_2(s_\Lambda^a, s_\Lambda^b) \sum_{s_{\Lambda_b}, s_\Lambda} H_m^1(s_{\Lambda_b}, s_\Lambda) \bar{H}_n^{1*}(s_{\Lambda_b}, s_\Lambda) \right) \\
& + (q^2 - 4m_l^2) \cdot L_{\mu\nu}^2 \cdot \left( \Gamma_2(s_\Lambda^a, s_\Lambda^b) \sum_{s_{\Lambda_b}, s_\Lambda} H_m^2(s_{\Lambda_b}, s_\Lambda) \bar{H}_n^{2*}(s_{\Lambda_b}, s_\Lambda) \right) \\
& + L_{\mu\nu}^3 \left( \Gamma_2(s_\Lambda^a, s_\Lambda^b) \sum_{s_{\Lambda_b}, s_\Lambda} H_m^1(s_{\Lambda_b}, s_\Lambda) \bar{H}_n^{2*}(s_{\Lambda_b}, s_\Lambda) \right) \\
& + L_{\mu\nu}^3 \left( \Gamma_2(s_\Lambda^a, s_\Lambda^b) \sum_{s_{\Lambda_b}, s_\Lambda} H_m^2(s_{\Lambda_b}, s_\Lambda) \bar{H}_n^{1*}(s_{\Lambda_b}, s_\Lambda) \right). \quad (3.20)
\end{aligned}$$

The complete description and possible terms are given in appendix C from equation C.6 to equation C.19. This equation can be written in terms of a set of trigonometric functions and angular coefficients after computing the leptonic and hadronic tensor in their respective frame of reference discussed in detailed in A.

$$\begin{aligned}
& \frac{d^4\Gamma}{dq^2 d \cos \theta_l d \cos \theta_\Lambda d\phi} = (K_{1ss} \sin^2 \theta_l + K_{1cc} \cos^2 \theta_l + K_{1c} \cos \theta_l) \\
& + (K_{2ss} \sin^2 \theta_l + K_{2cc} \cos^2 \theta_l + K_{2c} \cos \theta_l) \cos \theta_\Lambda \\
& + (K_{3sc} \sin \theta_l \cos \theta_l + K_{3s} \sin \theta_l) \sin \phi \sin \theta_\Lambda \\
& + (K_{4sc} \sin \theta_l \cos \theta_l + K_{4s} \sin \theta_l) \cos \phi \sin \theta_\Lambda. \quad (3.21)
\end{aligned}$$

### 3.4 Observable Calculations

For a particular decay the measurable quantities associated are term as "observable". Angular observable are determined experimentally and they are combination of the helicity amplitudes. These observable are developed such that it minimises theoretical uncertainty arises from form factor presence in helicity amplitude. This might be a measurement of, the branching ratio, or a lifespan, forward -backward asymmetry etc. A multi-body decay can have many observables, but a two-body decay will only have a small number of observable. For our decay the observable that we calculated are the following

- Branching Ratio

The integration equation from which the differential branching ratio is derived as, are;

$$\frac{d\beta}{dq^2} = \int_0^{2\pi} \int_0^\pi \int_0^\pi \frac{d^2\Gamma}{dq^2 d \cos \theta_l d \cos \theta_\Lambda d\phi} (\sin \theta_l \sin \theta_\Lambda) d\theta_l d\theta_\Lambda d\phi, \quad (3.22)$$

where the formulae are also derived from two fold distribution or angular coefficient in [11] as,

$$\frac{d\beta}{dq^2} = 2\hat{K}_{1ss} + \hat{K}_{1cc}. \quad (3.23)$$

- Longitudinal Polarization Fraction  $F_L$

The normalized longitudinal fraction is obtained from four fold distribution in equation 3.21 as follow [11],

$$F_L = 2\hat{K}_{1ss} - \hat{K}_{1cc}, \quad (3.24)$$

where hat means that each angular coefficient is normalized with branching ratio  $\frac{d\beta}{dq^2}$ .

$$\hat{K}_i = \frac{K_i}{2\hat{K}_{1ss} + \hat{K}_{1cc}}. \quad (3.25)$$

- Not only does it describe the well-known forward-backward asymmetry of the lepton side, we have following formulae

$$A_{FB}^l = \frac{3}{2}\hat{K}_{1c}. \quad (3.26)$$

- While the hadron side forward-backward asymmetry is

$$A_{FB}^\Lambda = \frac{1}{2}(2\hat{K}_{2ss} + \hat{K}_{2cc}). \quad (3.27)$$

- And the combined forward-backward asymmetry is defined as

$$A_{FB}^{\Lambda l} = \frac{3}{4}\hat{K}_{2c}. \quad (3.28)$$

- We also analyze the angular observable

$$\hat{K}_{4sc} = \frac{K_{4sc}}{2K_{1ss} + K_{1cc}}, \quad (3.29)$$

$$\hat{K}_{4s} = \frac{K_{4s}}{2K_{1ss} + K_{1cc}}, \quad (3.30)$$

$$\hat{K}_{2ss} = \frac{K_{2ss}}{2K_{1ss} + K_{1cc}}, \quad (3.31)$$

$$\hat{K}_{2cc} = \frac{K_{2cc}}{2K_{1ss} + K_{1cc}}. \quad (3.32)$$

### 3.4.1 Uncertainty Calculation

The decay rate, although being an essential observable, is impacted by uncertainties resulting from several input parameters, with form factors being the main contributors. The approach we outlined in our study to estimate the central values, statistical and systematic uncertainties for any observable is taken from [5] are as follow,

- Any observable's uncertainty determined by nominal fit form factor containing  $a_0$  and  $a_1$  given in equation D.2 in D.2. The central value of any observable and its uncertainty determined by nominal fit are indicated respectively as,

$$\mathcal{O}, \sigma_{\mathcal{O}}. \quad (3.33)$$

- Any observable's uncertainty determined by higher order fit form factor containing  $a_0$ ,  $a_1$  and  $a_2$  given in equation D.3 in appendix D.2. Any observable's central value at higher order fit and the uncertainty at higher order fit are indicated respectively as,

$$\mathcal{O}_{\text{OH}}, \sigma_{\mathcal{O},\text{OH}}. \quad (3.34)$$

- The systematic and statistical uncertainty are defined and calculated as follow,

$$\sigma_{\text{sys}} = \sigma_{\mathcal{O}}, \quad (3.35)$$

$$\sigma_{\text{stat}} = \max \left[ |\mathcal{O}_{\text{OH}} - \mathcal{O}|, \sqrt{|\sigma_{\mathcal{O},\text{OH}}^2 - \sigma_{\mathcal{O}}^2|} \right]. \quad (3.36)$$

- By adding the squares of each observable and calculating the square root of the sum, the uncertainty in central value of each observable is determined.

$$\sigma_{\text{Total}} = \sqrt{\sigma_{\text{stat}}^2 + \sigma_{\text{sys}}^2}. \quad (3.37)$$

- Any observable with a nominal fit parameter's total uncertainty central value is obtained by adding and subtracting the corresponding  $\sigma_{\text{Total}}$

$$\mathcal{O} \pm \sigma_{\text{Total}}.$$

## Chapter 4

# Numerical Analysis

*First, we present the numerical value we used for decay of  $\Lambda_b \rightarrow \Lambda(\rightarrow N\pi)l^+l^-$ . We begin by findings result for the Standard Model (SM). Next, we provide two New Physics (NP) scenarios using the model-independent approach. We compare our theoretical graphs with experimental data to finish our analysis. We presented the experimental data, NP analysis, and the SM derived values for each observable in our study.*

We give the numerical analysis for the aforementioned observables that are discussed in previous section i.e. branching ratio, lepton forward-backward asymmetry etc. We provide both predictions from the standard model and conduct an analysis of new physics that is not model-dependent. Additionally, we have generated experimental data plots illustrating observations for certain measurable quantities. The input parameter numerical values such as masses  $m_l$ ,  $\lambda_t$ ,  $m_{\Lambda_b}$ ,  $m_\Lambda$  etc are used given in table 4.1. The wilson co-efficient, that we have used for our calculation are given in [4] and numerical formulae are given in Appendix C. Our main objective is to study the differential decay width and other observable in  $\Lambda_b \rightarrow \Lambda(\rightarrow N\pi)l^+l^-$  in SMEFT and also the effect of new physics on it and match it with the experimental results.

Table 4.1: Values of the used input parameters.

Constant	Values	Constant	Values
$G_F$	$1.166378 \times 10^{-5} \text{ GeV}^{-2}$	$ V_{tb}V_{ts}^* $	$0.0397_{-0.0006}^{+0.0008}$
$m_b$	$4.18_{-0.02}^{+0.03} \text{ GeV}$	$\alpha(m_b)$	$1/133.28$
$\alpha_s(m_b)$	$0.2233$	$m_e$	$0.0005 \text{ GeV}$
$m_\mu$	$0.106 \text{ GeV}$	$m_{\text{pole}}$	$4.91 \pm 0.12 \text{ GeV}$
$m_\mu^{\text{MC}}$	$1.77 \pm 0.14 \text{ GeV}$	$\mu_b$	$5 \text{ GeV}$
$m_{A_s}$	$5.619 \text{ GeV}$	$m_A$	$1.116 \text{ GeV}$
$\tau_{A_b}$	$(1.471 \pm 0.009) \times 10^{-12} \text{ s}$		

For standard model calculation of the wilson co-efficient are given in Appendix C. The leading term that contribute in the calculation come from the  $C_9$ ,  $C_7$  and  $C_{10}$ . These short distance contributor are obtained using perturbative method in QCD. The new physics effects in semileptonic decay can be induced in two ways:

- One case we change operator basis same and change the wilson co-efficient only.
- Other case we can add new operators too.

Model independent approach, is used where all the possible operator (dimension-5 and dimension-6) are discuss within the standard model and its effect is also studied beyond standard model.

In our study we have only used the vector and axial vector operator and its chirality flipped counterpart are used that may be relevant to the new physics. The most general form of the effective Hamiltonian contains 10 local four fermion interactions which can contribute to the decay .

By adding NP effect only contribution come from semi leptonic electroweak penguin operator that contain  $C_9$  and  $C_{10}$ . Within NP the LFU and LFVU are also taken in account. The central value for these observable are shown in blue. The red band shows uncertainty upto  $1\sigma$  that arises due to form factors parameter we discussed earlier. The green line shows the new physics scenarios-8 with new physics wilson co-efficient used discussed in section 4.2. The purple line shows the new physics scenarios-11 with new physics wilson co-efficient used discussed in section 4.2. The uncertainty provided for the Standard-Model predictions is the overall uncertainty, which includes the statistical and systematic uncertainty from the form factors (propagated to the observable using the procedure explained in previous section).

#### 4.1 SM Results for $\Lambda_b \rightarrow \Lambda(\rightarrow N\pi)l^+l^-$

We calculated the numerical results for branching ratio  $\frac{d\beta}{dq^2}$ , fraction of longitudinal polarized dilepton  $F_L$ , lepton forward-backward asymmetry's  $A_{FB}^l$ , lepton-hadron forward-backward asymmetry's  $A_{FB}^{l\Lambda}$ , hadron forward-backward asymmetry's  $A_{FB}^\Lambda$ , along with other observable such as  $\hat{K}_{2ss}$ ,  $\hat{K}_{2cc}$ ,  $\hat{K}_{4s}$ , and  $\hat{K}_{4sc}$ . The numerical results of all these observable for Low s ranges from  $s = s_{min} = 0.102\text{GeV}^2$  to  $s = 8$ , and high s ranges from  $s = 15\text{GeV}^2$  to  $s = s_{max} = 20.21\text{GeV}^2$  within the SM are shown in figures 4.7. All  $\Lambda_b \rightarrow \Lambda(\rightarrow N\pi)l^+l^-$  angular observables are given as a function of dilepton invariant mass square  $q^2$  calculated in the Standard Model. The bands correspond to the uncertainties arises as explained in 4. The uncertainty in standard model and new physics are calculated upto  $1\sigma$ .

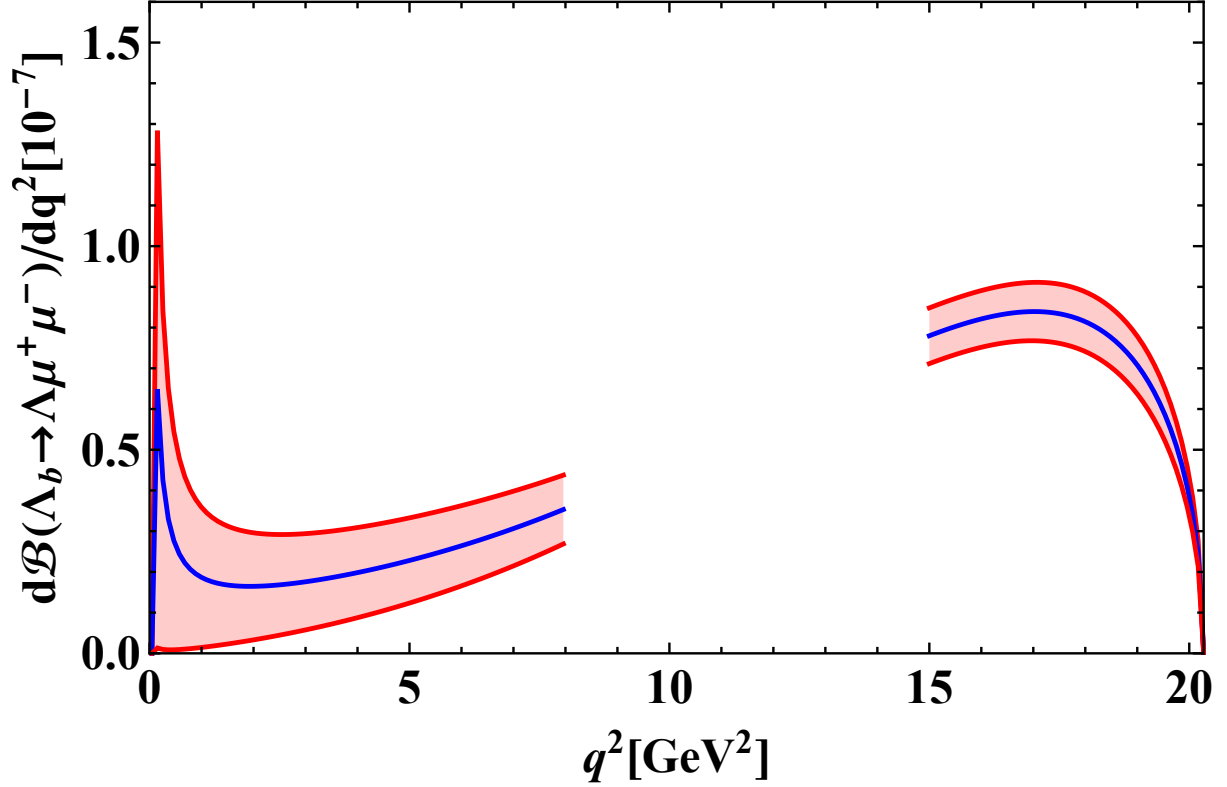


Figure 4.1: Differential Branching Fraction  $\frac{d\mathcal{B}}{dq^2}$ .

- $\frac{d\mathcal{B}}{dq^2}(q^2)$ : The  $\Lambda_b \rightarrow \Lambda(\rightarrow N\pi)l^+l^-$  decay mode branching ratio is seen to be  $\mathcal{O}(10^{-7})$ . The central value at  $s = 2$  is  $0.16 \times 10^{-7}\text{GeV}^2$  and at  $s = 8$ , value is  $0.335 \times 10^{-7}\text{GeV}^2$  and for high  $s$  at  $s = 15$  value is  $0.79 \times 10^{-7}\text{GeV}^2$ . The central values are shown in purple. The yellow line show maximum and minimum uncertainty calculation in our final expression in branching fraction. The bands in the graph include all value that lie within the calculation. Our result are comparable with other literature data [2], [10], [4]. The Branching ratio calculated in SM are given in equation 3.23



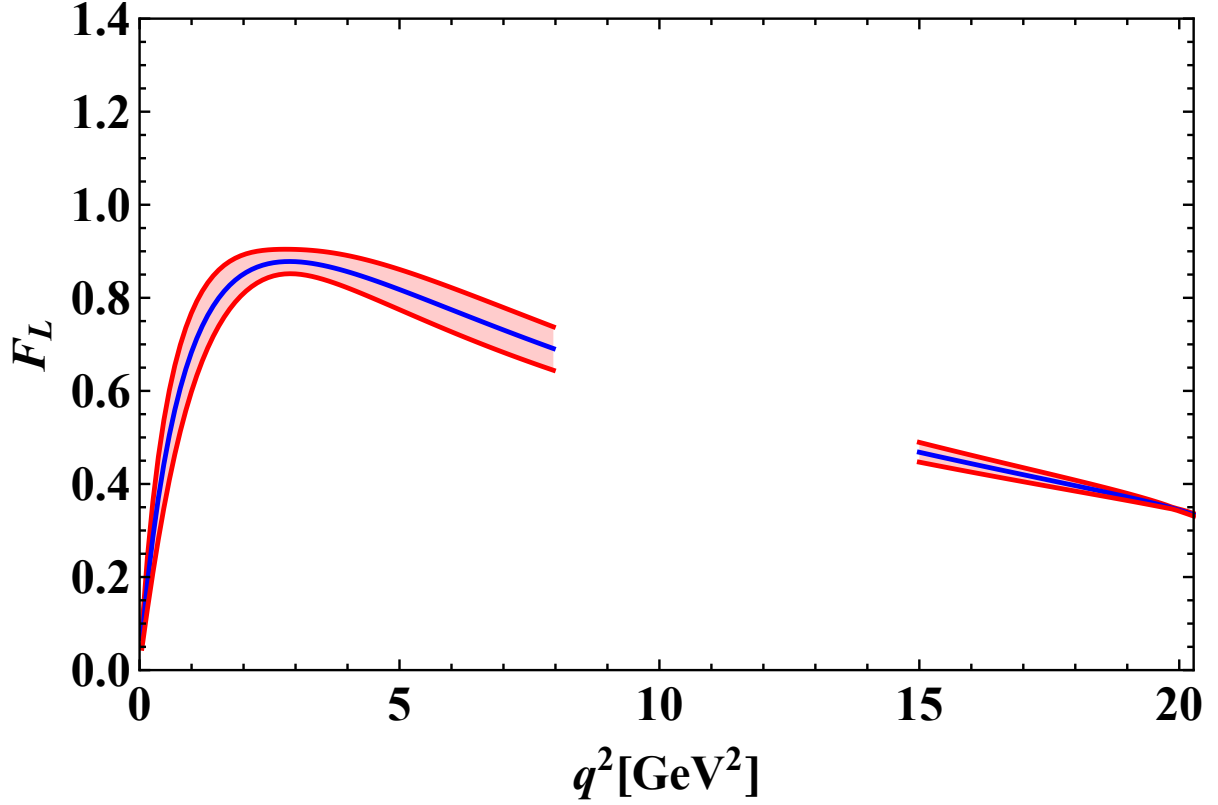


Figure 4.2: Longitudinal polarization fraction of di-leptons ( $F_L$ ).

- $F_L(q^2)$ : The  $\Lambda_b \rightarrow \Lambda(\rightarrow N\pi)l^+l^-$  decay mode di-lepton longitudinal polarization is seen to be  $0.851\text{GeV}^2$  at  $s = 2$ . At  $s = 8$   $F_L$  has value of  $0.689\text{GeV}^2$ . For high  $s$  the di-leptonic polarization observable has value of  $0.476\text{GeV}^2$  at  $s = 15$  and  $0.417\text{GeV}^2$  at  $s = 18$ . There is significant deviation for uncertainty band calculation arises from the form factor. Our results are comparable with other literature data [2], [10], [4]. The  $F_L$  calculated in SM are given

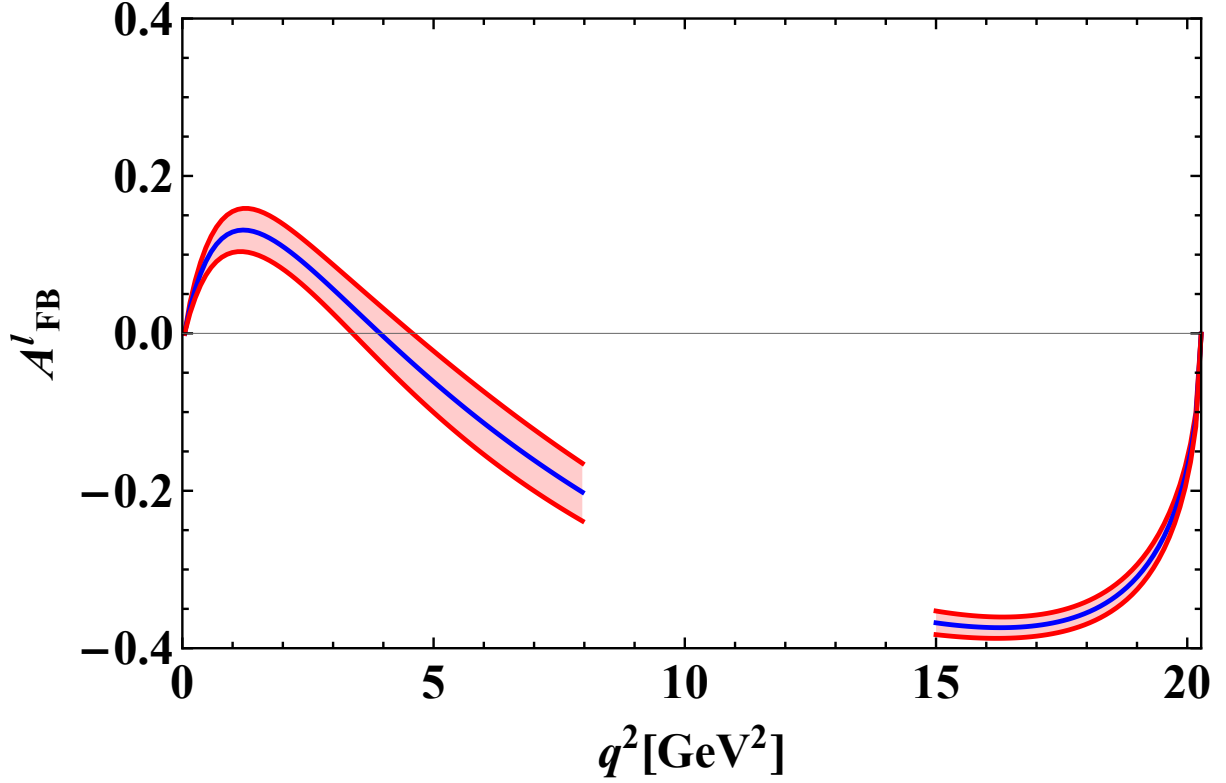


Figure 4.3: Lepton Forward-Backward Asymmetry ( $A_{FB}^1$ ).

- $A_{FB}^1(q^2)$ : The  $\Lambda_b \rightarrow \Lambda(\rightarrow N\pi)l^+l^-$  decay mode lepton forward backward asymmetry is seen to be  $0.110\text{GeV}^2$  at  $s = 2$  and  $-0.20\text{GeV}^2$  at  $s = 8$ . In high  $s$  region our calculated value for  $s = 15$  and  $s = 18$  are  $-0.361\text{GeV}^2$  and  $-0.342\text{GeV}^2$  respectively. The uncertainty band is wider for low  $s$  and thinner for high  $s$  in our calculated results. Our result are comparable with other literature data [2], [10], [4]. The  $A_{FB}^1$  calculated in SM are given

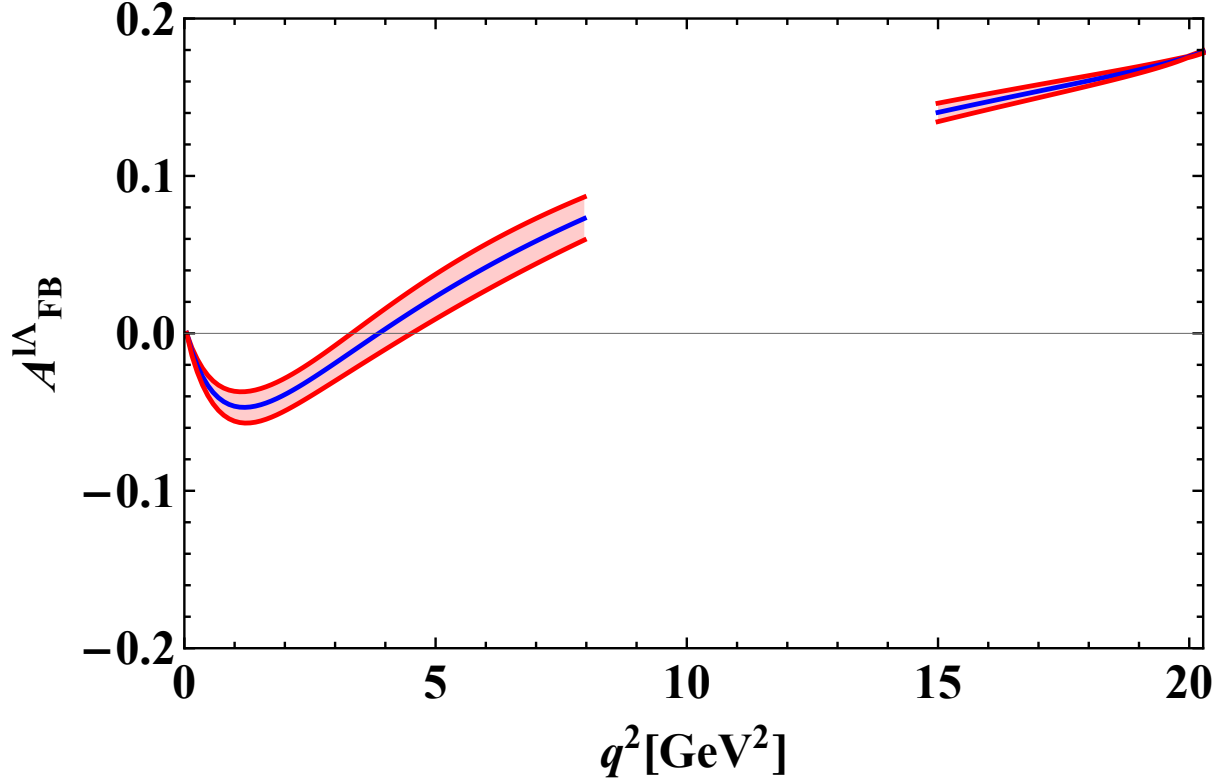


Figure 4.4: Lepton Hadron Forward Backward Asymmetry ( $A_{FB}^{\Lambda}$ ).

- $A_{FB}^{\Lambda}(q^2)$ : The  $\Lambda_b \rightarrow \Lambda(\rightarrow N\pi)l^+l^-$  decay mode lepton hadron forward backward asymmetry is seen to be  $-0.038\text{GeV}^2$ ,  $-0.018\text{GeV}^2$  and  $0.073\text{GeV}^2$  at  $s = 2$ ,  $s = 3$  and  $s = 8$  respectively. Analogous to lepton forward backward asymmetry there is zero crossing point in this observable. Our result are comparable with other literature data [2], [10], [4]. The  $A_{FB}^{\Lambda}$  calculated in SM are given

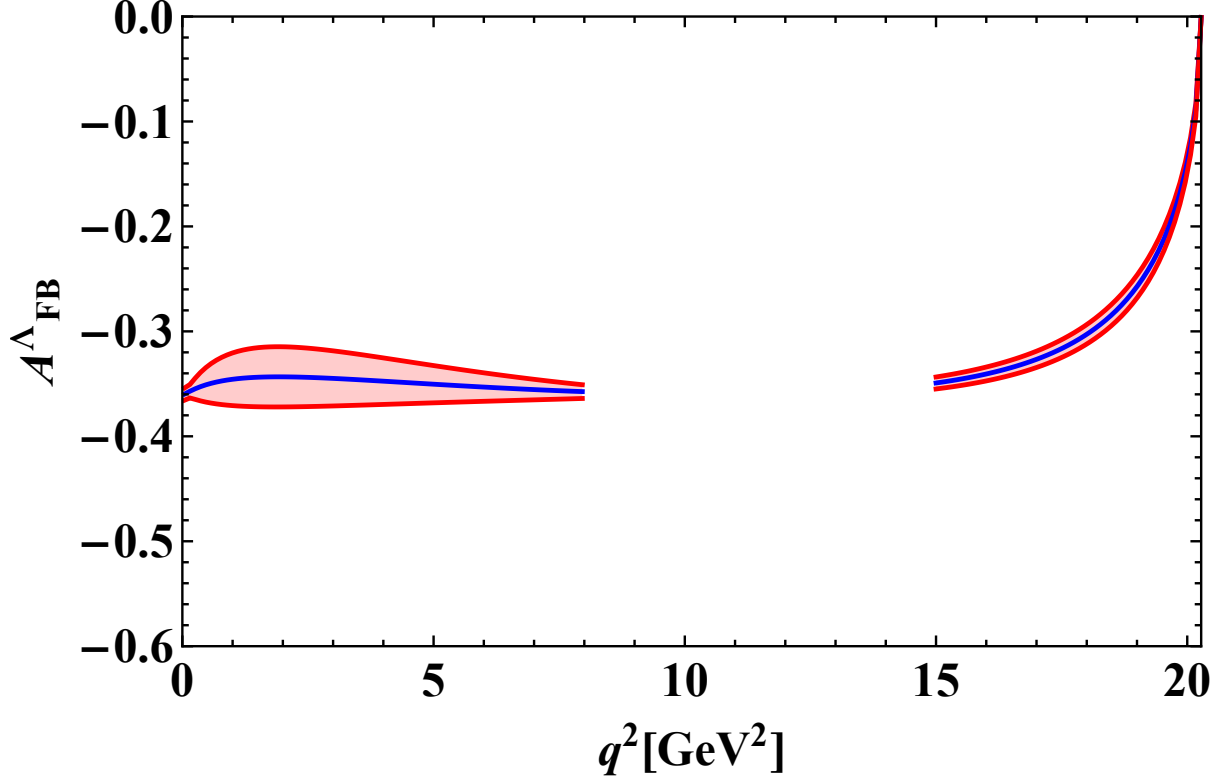


Figure 4.5: Hadron Forward Backward Asymmetry ( $A_{FB}^{\Lambda}$ ).

- $A_{FB}^{\Lambda}(q^2)$ : The  $\Lambda_b \rightarrow \Lambda(\rightarrow N\pi)l^+l^-$  decay mode lepton hadron forward backward asymmetry is seen to be  $-0.328\text{GeV}^2$ ,  $-0.334\text{GeV}^2$  and  $0.354\text{GeV}^2$  at  $s = 2$ ,  $s = 3$  and  $s = 8$  respectively. For high  $s$  otherwise the value are all below zero for example for  $-0.337\text{GeV}^2$  at  $s = 15$  and  $0.279\text{GeV}^2$  at  $s = 18$ . All the result are comparable with other literature data [2], [10], [4]. The  $A_{FB}^{\Lambda}$  calculated in SM are given

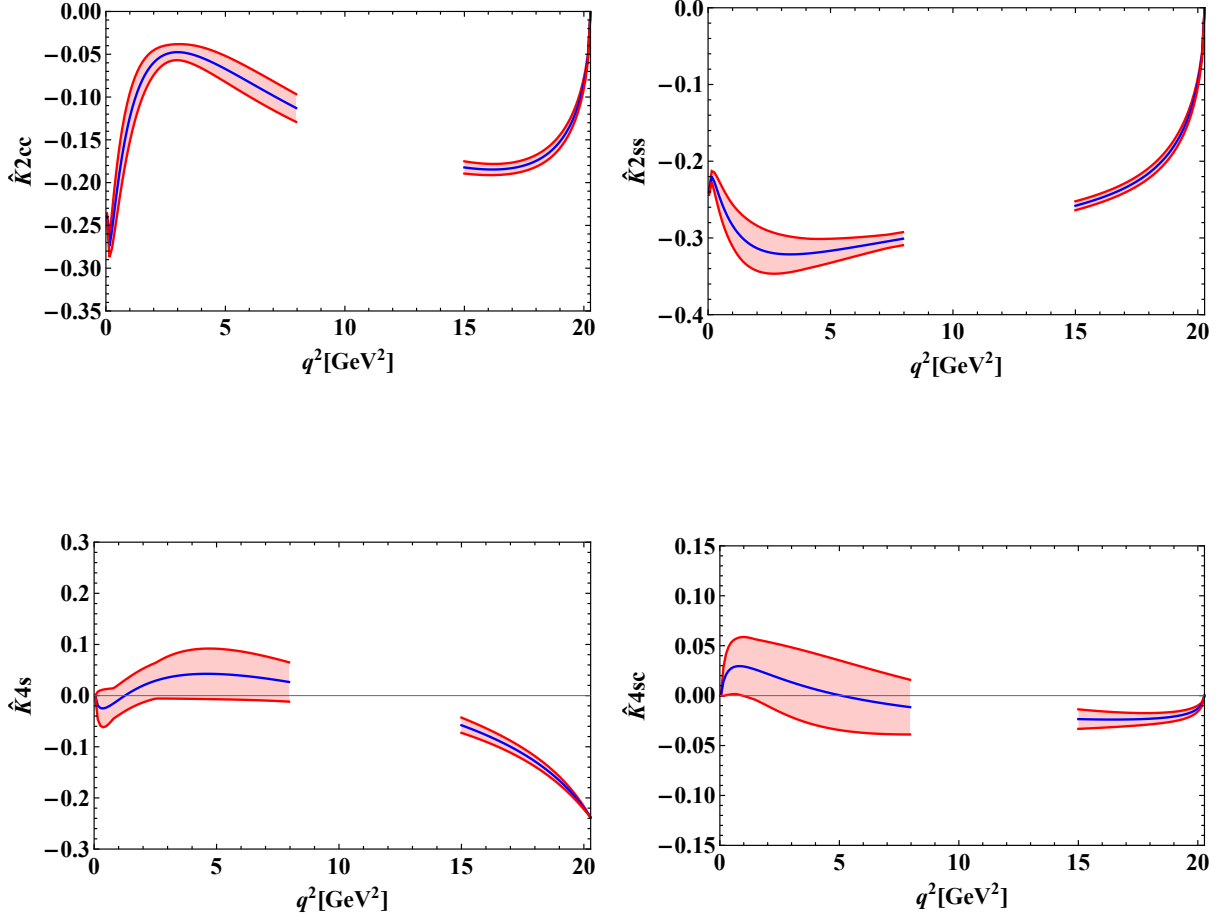


Figure 4.6: SM Results for  $\hat{K}_{2ss}$ ,  $\hat{K}_{2cc}$ ,  $\hat{K}_{4sc}$ , and  $\hat{K}_{4s}$ .

- $\hat{K}_{2ss}$ ,  $\hat{K}_{2cc}$ ,  $\hat{K}_{4s}$  and  $\hat{K}_{4sc}$ : In line with these asymmetries, we have also performed calculations for  $\hat{K}_{2ss}$ ,  $\hat{K}_{2cc}$ ,  $\hat{K}_{4sc}$ , and  $\hat{K}_{4s}$ . The central value are shown in blue and band in yellow which corresponds to uncertainty in form factors. For first observable  $\hat{K}_{2cc}$  numerical value at  $s = 2$ ,  $s = 8$ ,  $s = 15$ , and  $s = 18$  are  $-0.049\text{GeV}^2$ ,  $-0.040\text{GeV}^2$ ,  $-0.179\text{GeV}^2$ , and  $-0.168\text{GeV}^2$  respectively. For second observable  $\hat{K}_{2ss}$  numerical value at  $s = 2$ ,  $s = 8$ ,  $s = 15$ , and  $s = 18$  are  $-0.303\text{GeV}^2$ ,  $-0.314\text{GeV}^2$ ,  $-0.247\text{GeV}^2$ , and  $-0.195\text{GeV}^2$  respectively. For third observable  $\hat{K}_{4s}$  numerical value at  $s = 2$ ,  $s = 8$ ,  $s = 15$ , and  $s = 18$  are  $0.019\text{GeV}^2$ ,  $0.026\text{GeV}^2$ ,  $-0.056\text{GeV}^2$ , and  $-0.124\text{GeV}^2$  respectively. For last observable  $\hat{K}_{4sc}$  numerical value at  $s = 2$ ,  $s = 8$ ,  $s = 15$ , and  $s = 18$  are  $0.021\text{GeV}^2$ ,  $-0.011\text{GeV}^2$ ,  $-0.040\text{GeV}^2$ , and  $-0.024\text{GeV}^2$  respectively. The uncertainty arises from the form factor are clearly shown in red and have broader error band for low  $q^2$  and thinner for high  $q^2$  region in all of four observable namely  $\hat{K}_{2ss}$ ,  $\hat{K}_{2cc}$ ,  $\hat{K}_{4s}$ , and  $\hat{K}_{4sc}$ .

## 4.2 NP results for $\Lambda_b \rightarrow \Lambda(\rightarrow N\pi)l^+l^-$

Our main task in this study was to investigate NP effect on  $\Lambda_b \rightarrow \Lambda(\rightarrow N\pi)l^+l^-$  decay. New physics effect appear in these type of decays through the Wilson coefficients via global fit

analysis or through complete new operator from model-independent approach. All numerical value and form factor equation remain the same in our calculation of NP. The semi leptonic decay channel describe by  $b \rightarrow sl^+l^-$  is very important because they consist of many observable that we discussed in the previous section. Studying these observable are very beneficial because they can provide a new testing ground for NP beyond the SM.

As all NP scenarios are expressed in term of wilson co-efficient at  $\mu = 4.8\text{GeV}^2$ . We have used these data from the global fit of the NP wilson co-efficient of electroweak theory via model independent approach. In [34], they have used three different framework for there calculation and we have taken their result in our calculation to look for NP effect in our observables. The NP and SM contribution are separated as  $C_i = C_i^{SM} + C_i^{NP} + C_i^{NP'}$ . The hypothesis we used we have split the NP and NP-primed contribution into lepton flavor universal (LFU) and lepton flavor universal violating (LFUV) contributions as,

$$C_i^{\text{NP}} = C_i^{\text{NPU}} + C_i^{\text{NPV}}, \quad (4.1)$$

$$C_i^{\text{NP}'} = C_i^{\text{NPU}'} + C_i^{\text{NPV}'}. \quad (4.2)$$

In the first scenario that we represent in green color the non zero co-efficient have numerical value  $C_9^{\text{NPU}} = -1.25$ ,  $C_9^{\text{NPV}} = -0.16$ , and  $C_{10}^{\text{NPV}} = 0.16$  and all other  $C_9^{\text{NPU}'} = C_9^{\text{NPV}'} = C_{10}^{\text{NPU}} = C_{10}^{\text{NPU}'} = C_{10}^{\text{NPV}'} = 0$ . In second scenario,  $C_9^{\text{NPV}} = -0.84$ , and  $C_{10}^{\text{NPU}'} = -0.15$  and all other  $C_9^{\text{NPU}'} = C_9^{\text{NPV}'} = C_{10}^{\text{NPV}} = C_{10}^{\text{NPU}} = C_{10}^{\text{NPV}'} = C_9^{\text{NPU}} = 0$ . The  $C_7$  co-efficient has no contribution in NP they remain the same as calculated for SM.

Table 4.2: Global fit values of Wilson coefficients.

Coefficient	Scenario 8	Scenario 11
$C_9^{\text{NPU}}$	-1.25	0
$C_9^{\text{NPV}}$	-0.16	-0.84
$C_{9'}^{\text{NPU}}$	0	0
$C_{9'}^{\text{NPV}}$	0	0
$C_{10}^{\text{NPU}}$	0	0
$C_{10}^{\text{NPV}}$	0.16	0
$C_{10'}^{\text{NPU}}$	0	-0.15
$C_{10'}^{\text{NPV}}$	0	0

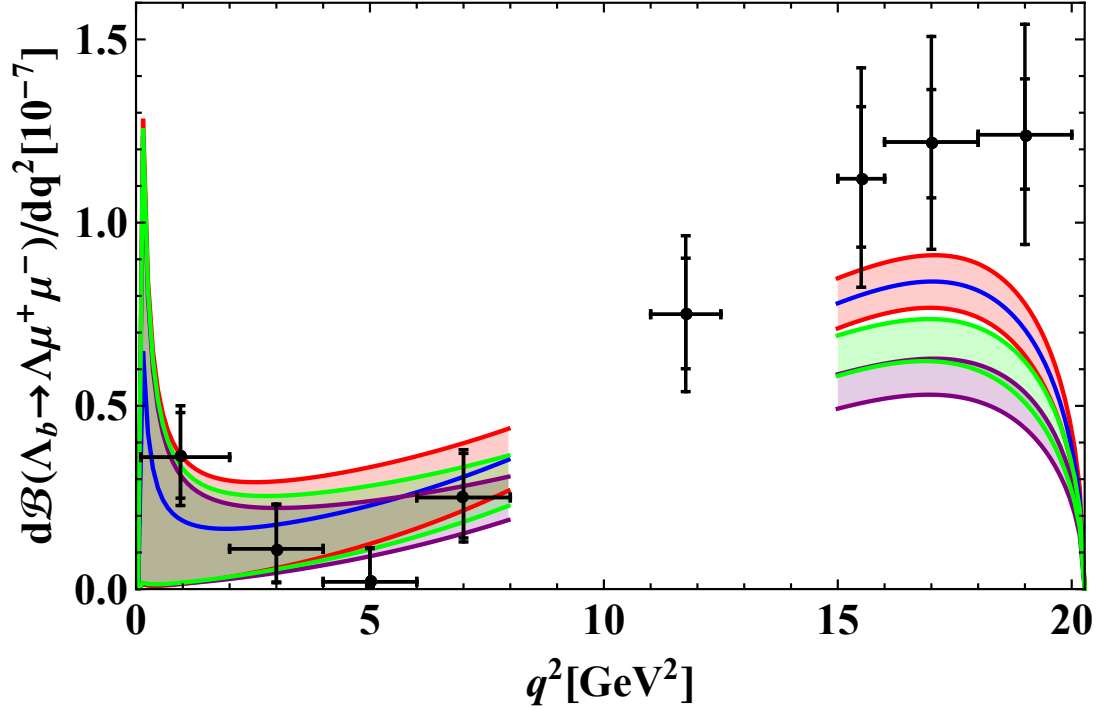


Figure 4.7: NP Results for Branching Fraction  $\frac{d\mathcal{B}}{dq^2}$ .

- The  $\Lambda_b \rightarrow \Lambda(\rightarrow N\pi)l^+l^-$  decay mode branching ratio in NP is seen to be reduced from our SM calculation. Two NP scenario are shown in red and green colour and the result variate from SM data. We have use data from scenario 8 and 11 of table 9 in [34]. The detailed of these scenario are given in [34]. The branching ratio result in NP for low s are clearly shown in red and blue. The blue graph with central value of the observable are the one which are subtracted from central value of NP. The added one in red are above the central blue plot. Band gap or error gap for SM and two NP scenario are clearly visible in figure. For high s two NP scenario values lie below the SM. The lower value for green and higher value for purple overlap with each other. Our result are comparable with other literature data [2], [10], [4]. For low s the result of SM and NP also match while for high s the NP lie below the SM.

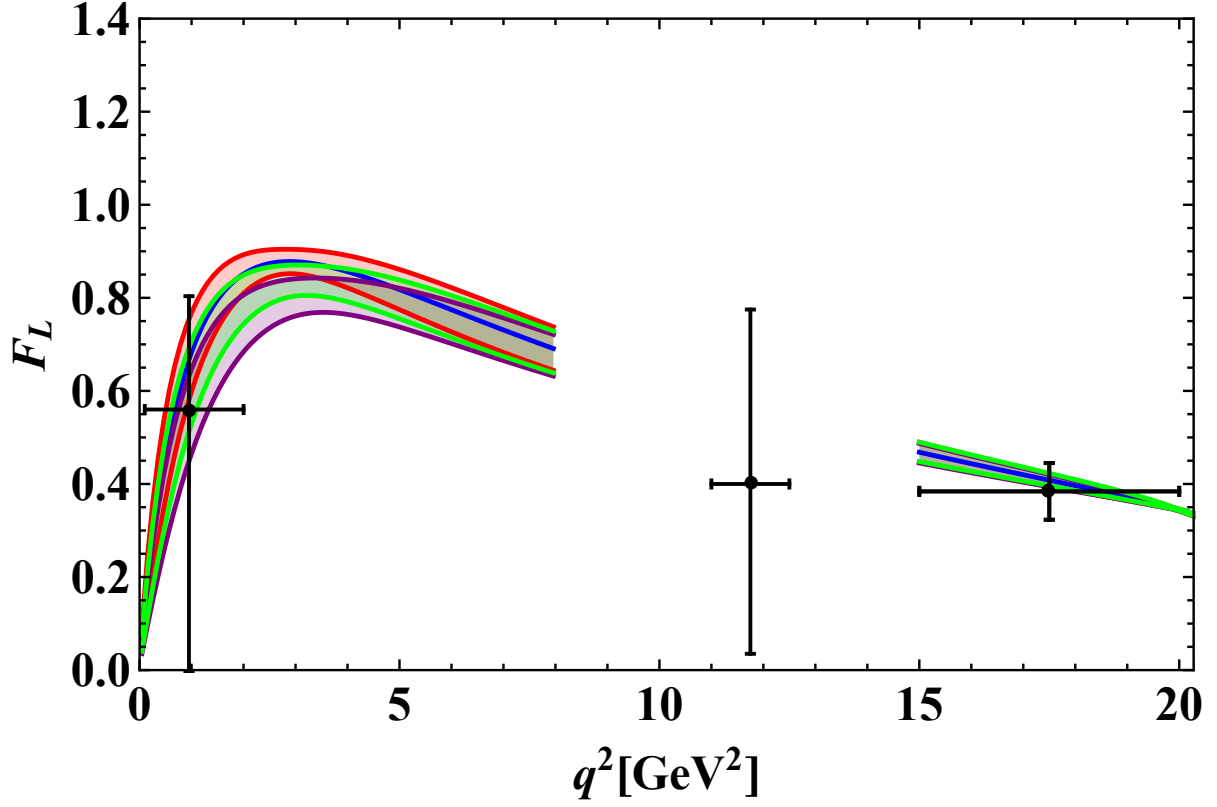


Figure 4.8: NP Results for the Longitudinal Polarization fraction of di-Leptons ( $F_L$ ).

- The  $\Lambda_b \rightarrow \Lambda(\rightarrow N\pi)l^+l^-$  decay mode Di-lepton longitudinal polarization is seen to be almost similar result for high  $s$ . Two NP scenario overlap with SM calculation for high  $s$ . For  $s$  value less than 8 there is small difference. Result for green lie below the central red plot while for purple they lie with in the SM error gap. Our result are comparable with other literature data [2], [10], [4]. The  $F_L$  calculated in SM and NP scenario are given in



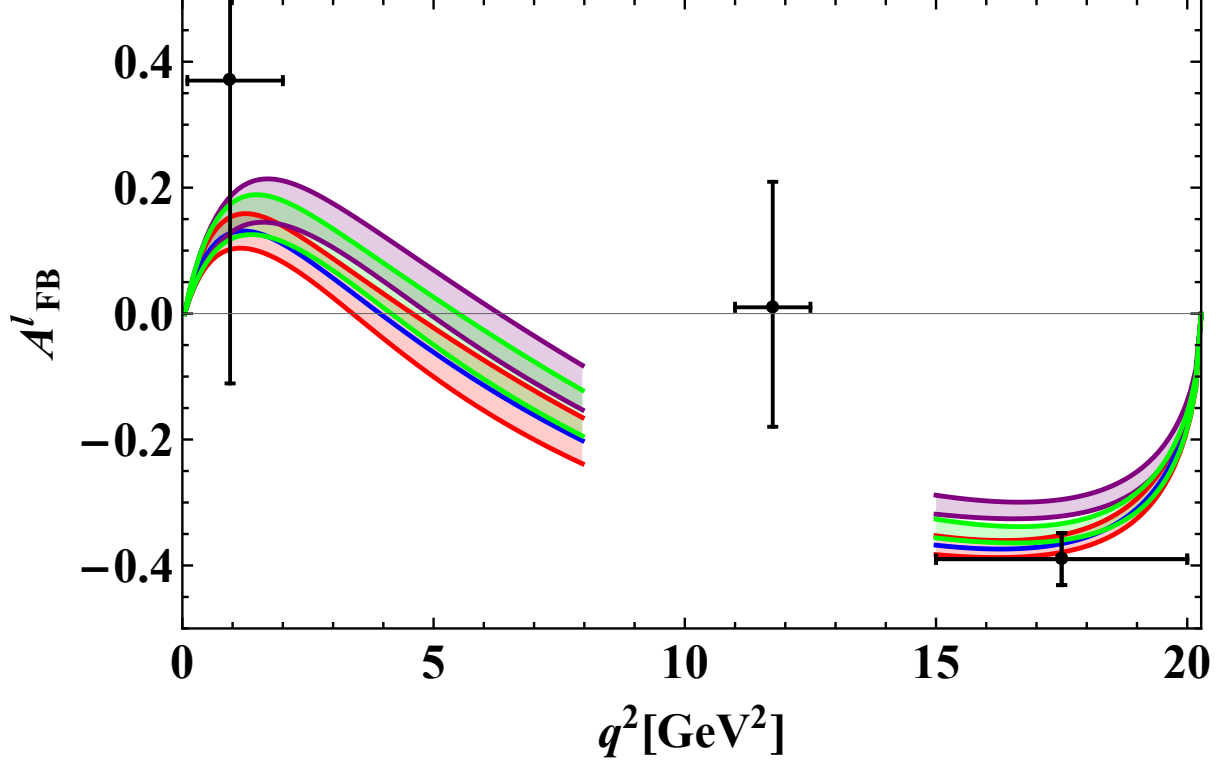


Figure 4.9: NP Results for Lepton Forward Backward Asymmetry ( $A'_{FB}$ ).

- The  $\Lambda_b \rightarrow \Lambda(\rightarrow N\pi)l^+l^-$  decay mode lepton forward backward asymmetry is seen to be reduced at low and high  $s$ . For SM the central value are given in the previous section. For this observable the NP scenario value are both above the central purple plots. The low  $s$  region for red plot almost overlap with the central value of the angular observable  $A'_{FB}$ . For high  $s$  the variation in SM and NP are quite different. The band gap for high  $s$  has less thickness and so for NP scenario. The purple are above the SM plot where green lower value overlap with the SM calculation. There is also zero crossing point in both NP calculation. Our result are comparable with other literature data [2], [10], [4]. The  $A'_{FB}$  calculated in SM and NP are given

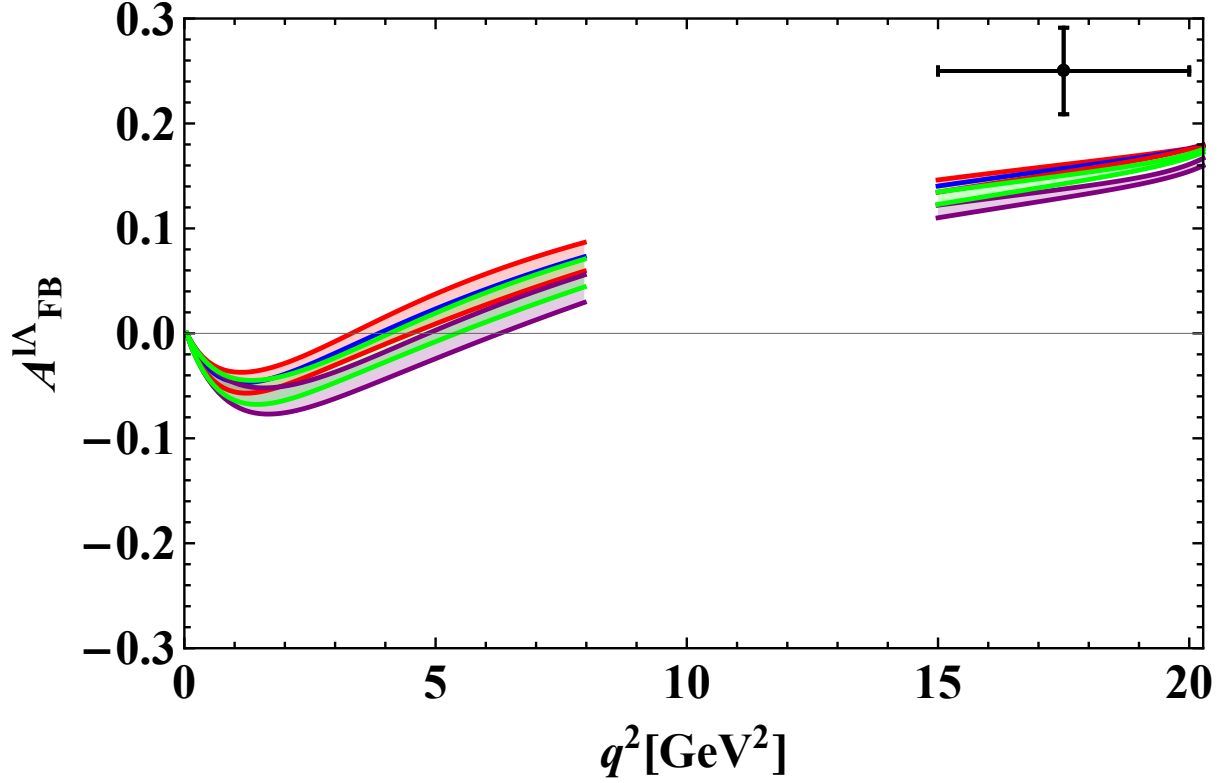


Figure 4.10: NP Results for Lepton Hadron Forward Backward Asymmetry ( $A_{FB}^{l\Lambda}$ ).

- The  $\Lambda_b \rightarrow \Lambda(\rightarrow N\pi)l^+l^-$  decay mode lepton hadron forward backward asymmetry is seen to be less difference between low and high  $s$ . NP calculation for low  $s$  lie below central value of  $A_{FB}^{l\Lambda}$  in SM. Calculation for purple overlap in the lower error region of SM. For green the error plot and their gaps lie below the SM calculated value. For high  $s$  the result have very clear variation between the SM calculation and NP. For high  $s$  all NP calculation reduced for all  $q^2$ . All the NP scenarios are distinguishable from the SM prediction at more than  $1\sigma$  in the high  $q^2$  region.

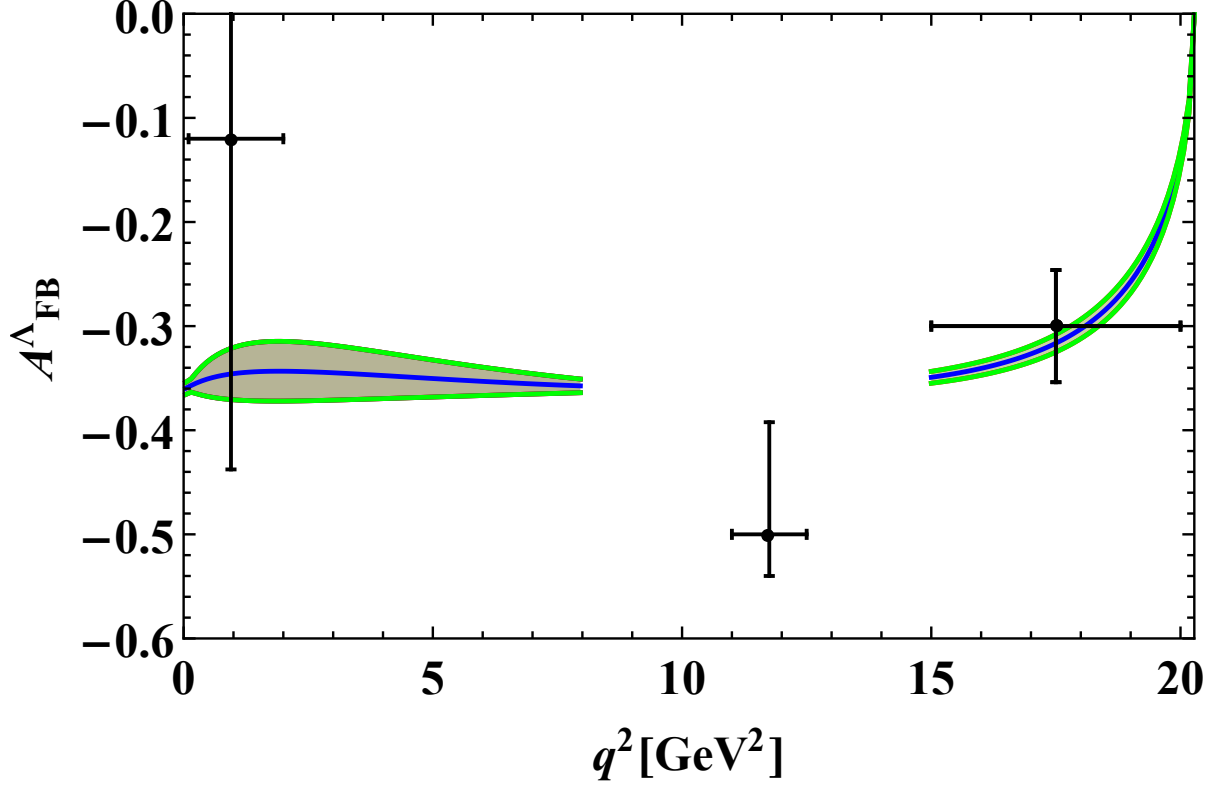


Figure 4.11: NP Results for Hadron Forward Backward Asymmetry ( $A_{FB}^{\Lambda}$ ).

- The  $\Lambda_b \rightarrow \Lambda(\rightarrow N\pi)l^+l^-$  decay mode hadron forward backward asymmetry in NP have almost similar result for all  $q^2$  region both the low and high. Our calculated value for low s region for example  $s = 2$ ,  $s = 3$ , and  $s = 8$  is  $-0.328\text{GeV}^2$ ,  $-0.334\text{GeV}^2$ , and  $-0.354\text{GeV}^2$  respectively. For high  $q^2$  region at  $s = 15$  is  $-0.337\text{GeV}^2$  and  $s = 18$  is  $-0.279\text{GeV}^2$ . For NP scenario that are describe in previous section the result are exactly similar to SM result both at low s and high s.

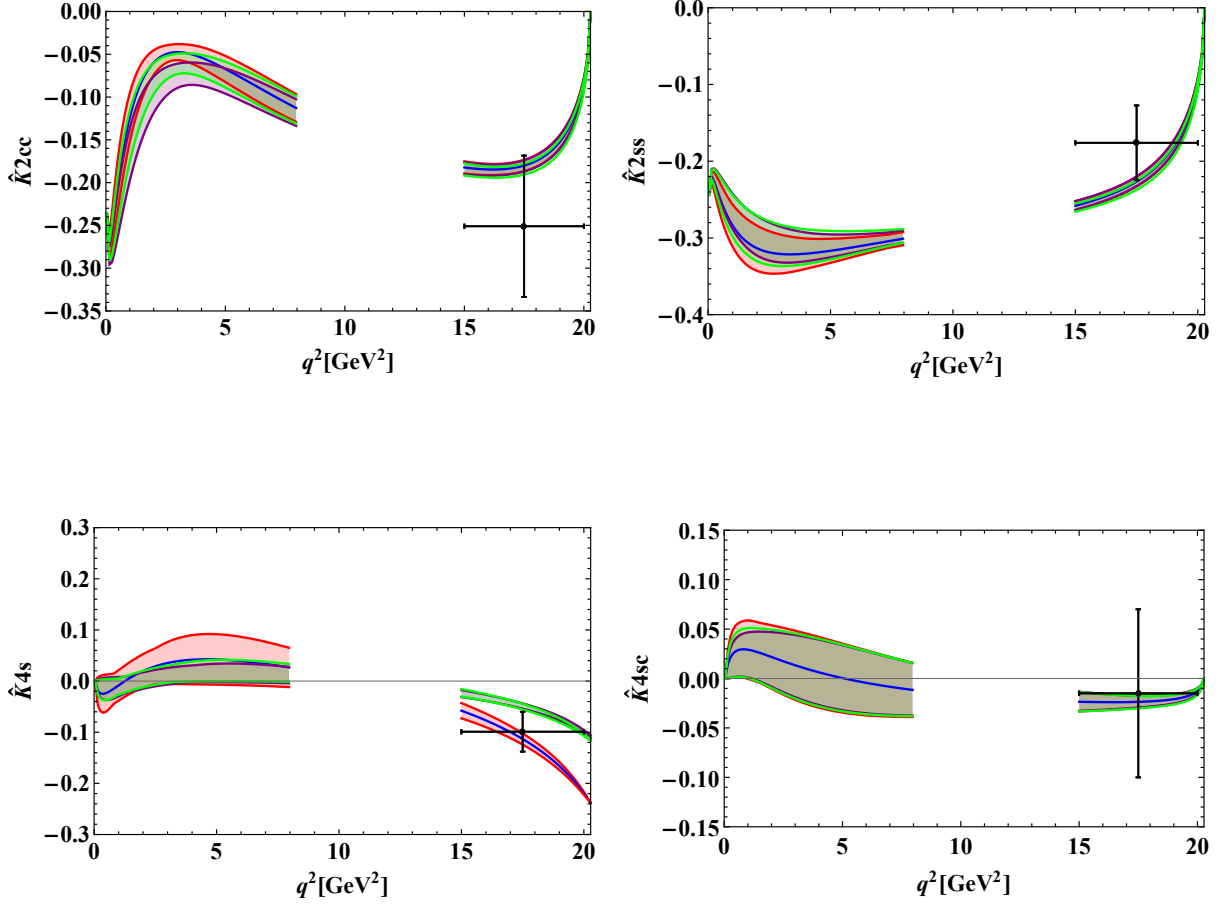


Figure 4.12: NP prediction for  $\hat{K}_{2ss}$ ,  $\hat{K}_{2cc}$ ,  $\hat{K}_{4sc}$ , and  $\hat{K}_{4s}$ .

- In addition with these asymmetries, we have also performed calculations in SM for four other observable. We incorporated NP scenario and find the following four observable and there variation from SM data. For  $K_{4sc}$  the NP and SM results completely matched. They overlap with each other and have no variation. For  $\hat{K}_{4s}$  the uncertainty band at low  $s$  is less than in the SM where at high  $s$  the NP result are higher and both the NP scenario overlap. For  $\hat{K}_{4s}$  the NP scenario results lie within the central plot of SM and the lower error plot in red. The  $\hat{K}_{2ss}$  and  $\hat{K}_{2cc}$  high  $s$  value for SM and NP are similar while for low  $s$  they are slightly different as shown in purple and green. For low region in  $q^2$  the NP scenario have slight variation from SM. For high  $q^2$  region three observable  $\hat{K}_{2ss}$ ,  $\hat{K}_{2cc}$ , and  $\hat{K}_{4sc}$  have exactly similar calculation and numerical value for both NP scenarios and SM.

## Chapter 5

# Conclusions

We have examined the four-fold differential decay distribution of the semi-leptonic  $\Lambda_b \rightarrow \Lambda(\rightarrow N\pi)l^+l^-$  decay. At the quark level the decay transition is from  $b \rightarrow s$  that are flavor changing neutral current transition. These FCNC transitions are forbidden at tree level, we move to one loop level, i.e. penguin diagram in our case. We have defined the kinematics of our decay and write down the hamiltonian from OPE. We get our final differential four fold decay distribution as follow,

$$\begin{aligned} \frac{d^4\Gamma}{dq^2 d\cos\theta_l d\cos\theta_\Lambda d\phi} = & (K_{1ss} \sin^2\theta_l + K_{1cc} \cos^2\theta_l + K_{1c} \cos\theta_l) \\ & + (K_{2ss} \sin^2\theta_l + K_{2cc} \cos^2\theta_l + K_{2c} \cos\theta_l) \cos\theta_\Lambda \\ & + (K_{3sc} \sin\theta_l \cos\theta_l + K_{3s} \sin\theta_l) \sin\phi \sin\theta_\Lambda \\ & + (K_{4sc} \sin\theta_l \cos\theta_l + K_{4s} \sin\theta_l) \cos\phi \sin\theta_\Lambda. \end{aligned} \quad (5.1)$$

The hamiltonian that we have used is obtained from OPE that divides it into two part i.e., short distance physics includes the wilson co-efficients and long distance part involves the local operators. The former are calculated within the SM via perturbative QCD from loop diagram where the later are obtained via non-perturbative QCD in this case lattice QCD is used. A 4-fold differential decay width of  $\Lambda_b \rightarrow \Lambda(\rightarrow N\pi)l^+l^-$  is obtained in two steps,  $\Lambda_b \rightarrow \Lambda l^+l^-$  followed by  $\Lambda(\rightarrow N\pi)$ . The four fold differential distribution equation is then obtained by multiplying both amplitude part of the decay with spin and polarization orientation taken in accordance with the kinematics of the decay.

The first step is obtaining the two fold distribution decay rate of  $\Lambda_b \rightarrow \Lambda$  transitions. The hadronic matrix element of this part is defined in helicity basis. We get ten  $q^2$  dependent form factor for this part describe in section 3.2.1. The non-zero helicity amplitude are written down for given spin orientation and spinor matrix element in equation 3.13. The form factors, which have been used are calculated using lattice QCD [35]. The Wilson co-efficients are taken from literature [18]. The two fold distribution  $\Lambda_b \rightarrow \Lambda l^+l^-$  is given in equation 3.18. Second step is calculating non zero helicity amplitudes of  $\Lambda(\rightarrow N\pi)$ . The detail is given in section 3.2.2. The final result that is shown in equation 5.1 is discussed in detailed in section 3.3.

For new physics we have used the standard effective field theory formalism with dimension six operators. The wilson co-efficient operator can in principle provides correlated NP effects in these observables. In order to obtain more accurate result for these observables, we also incorporated the NP result in our final expression and saw its effect on the listed observables [3]. NP scenarios are expressed through contributions to the Wilson coefficients and global fits analysis is used to assess which scenarios can describe the pattern of deviations observed. For each of these co-efficient, we have employed NP and NP primed part and also addition of lepton flavor universality and lepton flavor universality violation as discussed in chapter 3. We have used recent data accumulated from paper [34], where NP scenarios contribute to vector and axial

vector current only.

Our main task was to investigate the difference between the standard model and NP scenario effect on the calculated observable i.e, branching ratio ( $\frac{d\beta}{dq^2}$ ), longitudinal polarization fraction of dilepton ( $F_L$ ), lepton forward backward asymmetry ( $A_{FB}^l$ ), hadron forward backward asymmetry ( $A_{FB}^\Lambda$ ), combined forward backward asymmetry ( $A_{FB}^{l\Lambda}$ ), ( $\hat{K}_{2cc}$ ), ( $\hat{K}_{2cc}$ ), ( $\hat{K}_{4sc}$ ), and ( $\hat{K}_{4c}$ ). These are all obtained using the four fold distribution decay equation, and the results within SM are computed in accordance with other literature. The final graphs display the contribution of NP together with its outcome on our computed observable, colored in red and green.

In conclusion, our study of  $b \rightarrow s$  quark transition, in decay of  $\Lambda_b \rightarrow \Lambda(\rightarrow N\pi)\ell^+\ell^-$ , provides significant insights into flavor-changing neutral currents and their potential to probe new physics beyond the Standard Model. While the Standard Model predicts these transitions to occur at loop-level with the exchange of  $W$  bosons, our model-independent analysis allows for the investigation of beyond the Standard Model occurrences by examining various observables. Deviations in angular observables like branching ratio, lepton forward-backward asymmetry etc, from the Standard Model predictions could reveal new physics. These deviations are crucial for identifying possible contributions from new heavy particles, thereby extending our understanding of fundamental interactions.

# Appendix A

## Detail on the Kinematics

In this part we describe the kinematics of the decay  $\Lambda_b \rightarrow \Lambda(\rightarrow N\pi)l^+l^-$  and also the polarization vector associated with each particle.

### A.1 Di-lepton rest frame

The angle  $\theta_l$  is defined as the angle between the leptons and the z-axis. The lepton system is decaying on the xz-axes. The four momentum in the  $\bar{l}l$ -CM frame are [9].

$$\begin{aligned} p_{11}^\mu &= \{+E_d, +p_l \sin(\theta_l) \cos(\phi), +p_l \sin(\theta_l) \sin(\phi), +p_l \cos(\theta_l)\}, \\ p_{12}^\mu &= \{+E_d, -p_l \sin(\theta_l) \cos(\phi), -p_l \sin(\theta_l) \sin(\phi), -p_l \cos(\theta_l)\}. \end{aligned} \quad (\text{A.1})$$

With  $E_d = \frac{d}{2}$ ,  $\beta_l = \sqrt{1 - \frac{4ml^2}{d^2}}$ , and  $p_l = \frac{d}{2}\beta_l$ . The polarization vector in this frame are defined as

$$\epsilon^\mu(0) = (0, 0, 0, 1), \epsilon^\mu(t) = (1, 0, 0, 0), \epsilon^\mu(\pm) = \frac{1}{\sqrt{2}}(0, \mp 1, -i, 0). \quad (\text{A.2})$$

### A.2 $\Lambda_b$ rest frame

The four momentum of  $\Lambda_b(p)$ ,  $\lambda(k)$  and  $J_{effective} \rightarrow l^+l^-$  are defined in the rest frame of  $\Lambda_b(p)$  as follow [9]

$$\begin{aligned} p^\mu &= (m_{\Lambda_b}, 0, 0, 0), \\ k^\mu &= (E_f, 0, 0, k), \\ q^\mu &= (q_0, 0, 0, -k). \end{aligned} \quad (\text{A.3})$$

where  $E_f = \left(\frac{m_{\Lambda_b}^2 + m_\Lambda^2 - q^2}{2m_{\Lambda_b}}\right)$ ,  $q_0 = \left(\frac{m_{\Lambda_b}^2 - m_\Lambda^2 + q^2}{2m_{\Lambda_b}}\right)$  and  $k = \sqrt{E_f^2 - m_\Lambda^2}$ . Polarization vector in  $\Lambda_b$  rest frame can be read as follow,

$$\begin{aligned} \epsilon^\mu(t) &= \frac{1}{\sqrt{q^2}}(q_0, 0, 0, k), \\ \epsilon^\mu(\pm) &= \frac{1}{\sqrt{2}}(0, \mp 1, -i, 0), \\ \epsilon^\mu(0) &= \frac{1}{\sqrt{q^2}}(k, 0, 0, q_0). \end{aligned} \quad (\text{A.4})$$

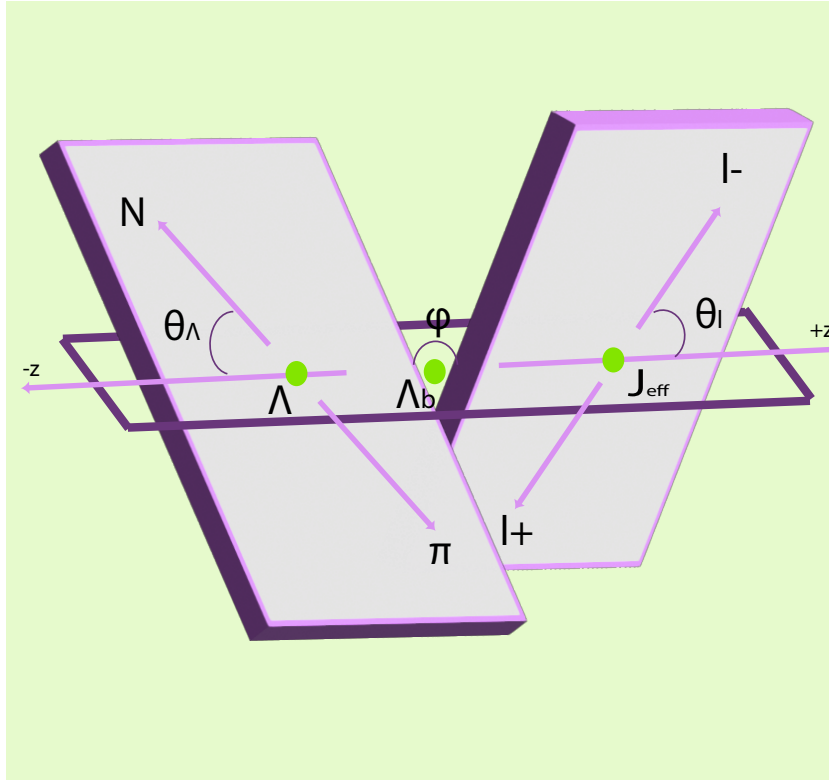


Figure A.1:  $\Lambda_b \rightarrow \Lambda(\rightarrow N\pi)l^+l^-$  decay kinematics with  $\theta_l$ ,  $\theta_\Lambda$  are angle between the  $z$ -axis and flight axis of Di-leptons and  $N\pi$  system respectively where  $\phi$  is azimuthal angle or angle between the plane of flights.



### A.3 $N\pi$ System

The invariant-mass-squared of  $N\pi$ -system is designated as  $m_\Lambda^2$ . Additionally, it may be distinguished by the azimuthal angle  $\phi$ , produced between the decay plane of the  $N\pi$ -system and that of  $l^+l^-$  the  $xz$ -plane. From the kinematics  $k_1$  and  $k_2$  is four momentum of  $N$  and  $\pi$  respectively and are

$$\begin{aligned} k_1^\mu &= (E_N, -k_N \sin \theta_\Lambda, 0, +k_N \cos \theta_\Lambda), \\ k_2^\mu &= (E_\pi, +k_N \sin \theta_\Lambda, 0, -k_N \cos \theta_\Lambda). \end{aligned} \quad (\text{A.5})$$

with the term defined as

$$\begin{aligned} |\vec{k}_N| &= \frac{\sqrt{\lambda(k^2, m_N^2, m_\pi^2)}}{2\sqrt{k^2}} \equiv \frac{\beta_{N\pi}}{2\sqrt{k^2}}, \\ \beta_{N\pi} &= \sqrt{\lambda\left(1, \frac{m_N^2}{k^2}, \frac{m_\pi^2}{k^2}\right)}, \\ E_N &= \frac{\sqrt{m_N^2 + \beta_{N\pi}^2 k^2}}{4}, \\ E_\pi &= \frac{\sqrt{m_\pi^2 + \beta_{N\pi}^2 k^2}}{4}. \end{aligned} \quad (\text{A.6})$$

The Källén function, defined as  $\lambda(a, b, c) = a^2 + b^2 + c^2 - 2(ab + ac + bc)$ .

### A.4 Partial Decay Rate

The general form of the Fermi golden rule is used to calculate the decay rate for two particle decay [36].

$$\Gamma_{fi} = \frac{1}{2M} \int |M_{fi}|^2 d\phi^2.$$

The decay's matrix component is called  $|M_{fi}|^2$ .  $d\phi^2$  is the phase space for two particle decay in the initial particle's rest frame and is given by [25],

$$d\phi^2 = (2\pi)^4 \delta(M - E_1 - E_2) \delta^3(p_1^2 + p_2^2) \frac{d^3 p_1}{2E_1 (2\pi)^3} \frac{d^3 p_2}{2E_2 (2\pi)^3}.$$

Where  $M$  is the mass of the initial particle, which will decay into two particles with  $p_1$  and  $p_2$  momentum in  $M$  rest frame. Now insert  $d\phi^2$  in decay rate equation

$$\Gamma_{fi} = \frac{1}{2M} \int |M_{fi}|^2 (2\pi)^4 \delta(M - E_1 - E_2) \delta^3(p_1^2 + p_2^2) \frac{d^3 p_1}{2E_1 (2\pi)^3} \frac{d^3 p_2}{2E_2 (2\pi)^3}.$$

Cancelling the same terms, we get,

$$\Gamma_{fi} = \frac{1}{8M\pi^2} \int |M_{fi}|^2 \delta(M - E_1 - E_2) \delta^3(p_1^2 + p_2^2) \frac{d^3 p_1}{2E_1} \frac{d^3 p_2}{2E_2}.$$

Evaluating the Dirac delta function in the above integral we get  $p_1 = -p_2$ ,  $\delta^3(p_1^2 + p_2^2)$  term will vanish the  $d^3p_2$  and we will get

$$\Gamma_{fi} = \frac{1}{2M} \int |M_{fi}|^2 \delta(M - E_1 - E_2) \frac{d^3p_1}{2E_1(2\pi)^2}.$$

As  $E_1^2 = m_1^2 + p_1^2$  and  $E_2^2 = m_2^2 + p_2^2$  and also from conservation of momentum  $p_1 = -p_2$ , so  $E_1^2 = m_1^2 + p_1^2$  and  $E_2^2 = m_2^2 + p_1^2$ , converting into spherical coordinate we get

$$d^3p_1 = p_1^2 \sin\theta dp_1 d\Phi = p_1^2 dp_1 d\Omega. \quad (\text{A.7})$$

Plug in equation we have now

$$\Gamma_{fi} = \frac{1}{2M(2\pi)^2} \int |M_{fi}|^2 \delta(M - E_1 - E_2) \frac{p_1^2 dp_1 d\Omega}{2E_1 2E_2}.$$

Putting value of  $E_1$  and  $E_2$  in the delta function we have

$$\Gamma_{fi} = \frac{1}{2M(2\pi)^2} \int |M_{fi}|^2 \delta(M - \sqrt{m_1^2 + p_1^2} - \sqrt{m_2^2 + p_1^2}) \frac{p_1^2 dp_1 d\Omega}{4E_1 E_2}.$$

This integral cannot be evaluated simply we will convert into functional form by putting

$$g(p_1) = \frac{p_1^2}{4E_2 E_1},$$

and also,

$$f(p_1) = M - \sqrt{m_1^2 + p_1^2} - \sqrt{m_2^2 + p_1^2},$$

we get,

$$\Gamma_{fi} = \frac{1}{2M(2\pi)^2} \int |M_{fi}|^2 \delta(f(p_1)g(p_1)) dp_1 d\Omega.$$

The  $(p_1)$  imposes the energy conservation on the equation and the term is only zero if  $p_1 = p^*$ . where is  $p^*$  solution of  $\delta(f(p^*))$ . The integral can be evaluated using the property of Dirac delta function.

$$\int |M_{fi}|^2 \delta(f(p_1)g(p_1)) dp_1 d\Omega = |M_{fi}|^2 g(p^*) \left| \frac{df}{dp_1} \right|^{-1},$$

$$\left| \frac{df}{dp_1} \right| = \frac{d(M - \sqrt{m_1^2 + p_1^2} - \sqrt{m_2^2 + p_1^2})}{dp_1},$$

$$\left| \frac{df}{dp_1} \right| = -\frac{p_1}{\sqrt{m_1^2 + p_1^2}} - \frac{p_1}{\sqrt{m_2^2 + p_1^2}},$$

$$\left| \frac{df}{dp_1} \right| = p_1 \left( \frac{1}{E_1} + \frac{1}{E_2} \right),$$

$$\left| \frac{df}{dp_1} \right| = p_1 \left( \frac{E_1 + E_2}{E_1 E_2} \right),$$

$$\left| \frac{df}{dp_1} \right|^{-1} = p_1 \left( \frac{E_1 E_2}{E_1 + E_2} \right),$$

$$g(p^*) = \frac{p_1^*}{4E_2 E_1},$$

we plug in the following equation

$$\Gamma_{fi} = \frac{1}{2M(2\pi)^2} \int |M_{fi}|^2 \delta(f(p_1)g(p_1)) dp_1 d\Omega,$$

$$\Gamma_{fi} = \frac{1}{2M(2\pi)^2} \int |M_{fi}|^2 \frac{1}{p_1^*} \frac{E_1 E_2}{E_1 + E_2} \frac{p_1^{2*}}{4E_1 E_2} d\Omega,$$

$$\Gamma_{fi} = \frac{1}{2M(2\pi)^2} \frac{p_1^*}{4M} \int |M_{fi}|^2 d\Omega. \quad (\text{A.8})$$

Hence the general expression for any two-body phase space is,

$$\frac{p_1^*}{32\pi^2 M^2} \int |M_{fi}|^2 d\Omega, \quad (\text{A.9})$$

$$p^* = \frac{1}{2} \sqrt{(M^2 - (m_1^2 + m_2^2))^2 (M^2 - (m_1^2 - m_2^2))^2}. \quad (\text{A.10})$$

## Appendix B

# Leptonic Tensor

For  $L_1^{\mu\nu} = p_{1\mu}p_{2\nu} + p_{2\mu}p_{1\nu}$  the possible non zero combination after contraction with the polarization vector of the dilepton system we have following formulae. Where all other combination are zero.

$$\begin{aligned}
p_{1\mu}\epsilon^\mu(0)p_{2\nu}\epsilon^{\dagger\nu}(0) + p_{2\mu}\epsilon^\mu(0)p_{1\nu}\epsilon^{\dagger\nu}(0) &= -\frac{1}{2}d^2\beta_l^2 \cos\theta_l, \\
p_{1\mu}\epsilon^\mu(0)p_{2\nu}\epsilon^{\dagger\nu}(\pm) + p_{2\mu}\epsilon^\mu(\pm)p_{1\nu}\epsilon^{\dagger\nu}(+) &= \pm\frac{1}{2\sqrt{2}}d^2\beta_l^2 \cos\theta_l \sin\theta_l e^{\mp i\phi}, \\
p_{1\mu}\epsilon^\mu(t)p_{2\nu}\epsilon^{\dagger\nu}(t) + p_{2\mu}\epsilon^\mu(t)p_{1\nu}\epsilon^{\dagger\nu}(t) &= \frac{d^2}{2}, \\
p_{1\mu}\epsilon^\mu(\pm)p_{2\nu}\epsilon^{\dagger\nu}(+\pm) + p_{2\mu}\epsilon^\mu(\pm)p_{1\nu}\epsilon^{\dagger\nu}(\pm) &= \pm\frac{1}{4}d^2\beta_l^2 \sin^2\theta_l, \\
p_{1\mu}\epsilon^\mu(\pm)p_{2\nu}\epsilon^{\dagger\nu}(0) + p_{2\mu}\epsilon^\mu(\pm)p_{1\nu}\epsilon^{\dagger\nu}(0) &= \pm\frac{1}{2\sqrt{2}}d^2\beta_l^2 \cos\theta_l \sin\theta_l e^{\pm i\phi}, \\
p_{1\mu}\epsilon^\mu(\pm)p_{2\nu}\epsilon^{\dagger\nu}(\mp) + p_{2\mu}\epsilon^\mu(\pm)p_{1\nu}\epsilon^{\dagger\nu}(\mp) &= \frac{1}{4}d^2\beta_l^2 \sin^2\theta_l e^{\pm 2i\phi}. \tag{B.1}
\end{aligned}$$

We have the following equations for  $L_2^{\mu\nu} = \iota\epsilon^{\alpha\beta\mu\nu}p_{1\alpha}p_{2\beta}\epsilon_\mu\epsilon_\nu^\dagger$ , which is the feasible non zero combination after contraction with the polarization vector of the dilepton system.

$$\begin{aligned}
\iota\epsilon^{\alpha\beta\mu\nu}p_{1\alpha}p_{2\beta}\epsilon_\mu(0)\epsilon_\nu^\dagger(\pm) &= \sqrt{2}d^2\beta_l \sin\theta_l e^{\mp i\phi}, \\
\iota\epsilon^{\alpha\beta\mu\nu}p_{1\alpha}p_{2\beta}\epsilon_\mu(\pm)\epsilon_\nu^\dagger(\pm) &= \mp 2d^2\beta_l \cos\theta_l, \\
\iota\epsilon^{\alpha\beta\mu\nu}p_{1\alpha}p_{2\beta}\epsilon_\mu(\pm)\epsilon_\nu^\dagger(0) &= -\sqrt{2}d^2\beta_l \sin\theta_l e^{\pm i\phi}. \tag{B.2}
\end{aligned}$$

For  $L_3^{\mu\nu} = \epsilon^\mu\epsilon^\nu g_{\mu\nu}$  the possible non zero combination after contraction with the polarization vector of the dilepton system we have following formulae. Where all other combination are zero.

$$\begin{aligned}
\epsilon^\mu(0)\epsilon^{\dagger\nu}(0)g_{\mu\nu} &= -1, \\
\epsilon^\mu(t)\epsilon^{\dagger\nu}(t)g_{\mu\nu} &= 1, \\
\epsilon^\mu(+)\epsilon^{\dagger\nu}(+)g_{\mu\nu} &= 1, \\
\epsilon^\mu(-)\epsilon^{\dagger\nu}(-)g_{\mu\nu} &= 1. \tag{B.3}
\end{aligned}$$

# Appendix C

## Hadronic Part

In this appendix we presented the spinor, current for  $\Lambda_b$  and  $\Lambda$  particle, and also the four fold helicity result.

### C.1 Hadronic Spinor Representation

We have utilized explicit formulas for the Dirac spinors that describe baryons with a particular momentum to compute the different helicity amplitudes.

$$u(p, s = +\frac{1}{2}) = \frac{1}{\sqrt{2}(p^0 + m)} \begin{bmatrix} +(p_0 + m - |\vec{p}|) \cos(\frac{\theta}{2}) \\ +(p_0 + m - |\vec{p}|) \sin(\frac{\theta}{2}) e^{+i\phi} \\ +(p_0 + m + |\vec{p}|) \cos(\frac{\theta}{2}) \\ +(p_0 + m + |\vec{p}|) \sin(\frac{\theta}{2}) e^{+i\phi} \end{bmatrix}, \quad (\text{C.1})$$

$$u(p, s = -\frac{1}{2}) = \frac{1}{\sqrt{2}(p^0 + m)} \begin{bmatrix} -(p_0 + m + |\vec{p}|) \sin(\frac{\theta}{2}) e^{-i\phi} \\ +(p_0 + m + |\vec{p}|) \cos(\frac{\theta}{2}) \\ -(p_0 + m - |\vec{p}|) \sin(\frac{\theta}{2}) e^{-i\phi} \\ +(p_0 + m - |\vec{p}|) \cos(\frac{\theta}{2}) \end{bmatrix}. \quad (\text{C.2})$$

### C.2 Hadronic Spinor Bilinears

In order to acquire the helicity amplitudes describing the transitions  $\Lambda_b \rightarrow \Lambda$  with scalar, pseudo scalar, vector, or axial vector currents, we obtained the following combination

$$\begin{aligned} u(k, \pm\frac{1}{2}) \bar{u}_b(p, \pm\frac{1}{2}) &= 0, \\ \bar{u}(k, \pm\frac{1}{2}) u_b(p, \mp\frac{1}{2}) &= \pm\sqrt{s_+}, \\ \bar{u}(k, \pm\frac{1}{2}) \gamma^5 u_b(p, \pm\frac{1}{2}) &= 0, \\ \bar{u}(k, \pm\frac{1}{2}) \gamma^5 u_b(p, \pm\frac{1}{2}) &= -\sqrt{s_-}. \end{aligned} \quad (\text{C.3})$$

and for vector and axial-vector currents, we obtain

$$\begin{aligned} \bar{u}(k, \pm\frac{1}{2}) \gamma^\mu u_b(p, \pm\frac{1}{2}) &= \mp\sqrt{2s_-} \epsilon^\mu(\pm), \\ \bar{u}(k, \pm\frac{1}{2}) \gamma^\mu u_b(p, \mp\frac{1}{2}) &= \pm(\sqrt{s_+}, 0, 0, -\sqrt{s_-}), \end{aligned}$$

$$\begin{aligned}\bar{u}(k, \pm \frac{1}{2})\gamma^\mu\gamma^5 u_b(p, \pm \frac{1}{2}) &= -\sqrt{2s_+}\epsilon^\mu(\pm), \\ \bar{u}(k, \pm \frac{1}{2})\gamma^\mu\gamma^5 u_b(p, \mp \frac{1}{2}) &= (\sqrt{s_-}, 0, 0, -\sqrt{s_+}).\end{aligned}\tag{C.4}$$

### C.3 Four Fold Distribution Final Spin Orientation

As we have derived our formulae for fold distribution on term of hadronic and leptonic helicity amplitude. The leptonic possible combination and their result are given in previous appendix. In this we have given detailed of hadronic spin and there possible non zero combination only from the kinematic describe in figure A.1. The equation can be changed if the kinematics of the particle changed but there should be no effect on the final expression of amplitude and all the observable that we have calculated. Let write the formulae and the result are just multiplied with the leptonic part in the end.

$$\Gamma_2(s_\Lambda^a, s_\Lambda^b) \sum_{s_{\Lambda_b}, s_\Lambda} H_m^i(s_{\Lambda_b}, s_\Lambda) \bar{H}_n^{j*}(s_{\Lambda_b}, s_\Lambda).\tag{C.5}$$

- $m = n = t,$

$$= \left( \Gamma_2(-\frac{1}{2}, -\frac{1}{2}) H_t^i(+\frac{1}{2}, -\frac{1}{2}) H_t^{j*}(+\frac{1}{2}, -\frac{1}{2}) + \Gamma_2(+\frac{1}{2}, +\frac{1}{2}) H_t^i(-\frac{1}{2}, +\frac{1}{2}) H_t^{j*}(-\frac{1}{2}, +\frac{1}{2}) \right).\tag{C.6}$$

- $m = t, n = 0,$

$$= \left( \Gamma_2(-\frac{1}{2}, -\frac{1}{2}) H_t^i(+\frac{1}{2}, -\frac{1}{2}) H_0^{j*}(+\frac{1}{2}, -\frac{1}{2}) + \Gamma_2(+\frac{1}{2}, +\frac{1}{2}) H_t^i(-\frac{1}{2}, +\frac{1}{2}) H_0^{j*}(-\frac{1}{2}, +\frac{1}{2}) \right).\tag{C.7}$$

- $m = t, n = +,$

$$= \left( \Gamma_2(-\frac{1}{2}, +\frac{1}{2}) H_t^i(+\frac{1}{2}, -\frac{1}{2}) H_+^{j*}(+\frac{1}{2}, +\frac{1}{2}) \right).\tag{C.8}$$

- $m = t, n = -,$

$$= \left( \Gamma_2(+\frac{1}{2}, -\frac{1}{2}) H_t^i(-\frac{1}{2}, +\frac{1}{2}) H_-^{j*}(-\frac{1}{2}, -\frac{1}{2}) \right).\tag{C.9}$$

- $m = 0, n = t,$

$$= \left( \Gamma_2(-\frac{1}{2}, -\frac{1}{2}) H_0^i(+\frac{1}{2}, -\frac{1}{2}) H_t^{j*}(+\frac{1}{2}, -\frac{1}{2}) + \Gamma_2(+\frac{1}{2}, +\frac{1}{2}) H_0^i(-\frac{1}{2}, +\frac{1}{2}) H_t^{j*}(-\frac{1}{2}, +\frac{1}{2}) \right).\tag{C.10}$$

- $m = n = 0,$

$$= \left( \Gamma_2(-\frac{1}{2}, -\frac{1}{2}) H_0^i(+\frac{1}{2}, -\frac{1}{2}) H_0^{j*}(+\frac{1}{2}, -\frac{1}{2}) + \Gamma_2(+\frac{1}{2}, +\frac{1}{2}) H_0^i(-\frac{1}{2}, +\frac{1}{2}) H_0^{j*}(-\frac{1}{2}, +\frac{1}{2}) \right).\tag{C.11}$$

- $m = 0, n = +,$

$$= \left( \Gamma_2\left(-\frac{1}{2}, +\frac{1}{2}\right) H_0^i\left(+\frac{1}{2}, -\frac{1}{2}\right) H_+^{j*}\left(+\frac{1}{2}, +\frac{1}{2}\right) \right). \quad (\text{C.12})$$

- $m = 0, n = -,$

$$= \left( \Gamma_2\left(+\frac{1}{2}, -\frac{1}{2}\right) H_0^i\left(-\frac{1}{2}, +\frac{1}{2}\right) H_-^{j*}\left(-\frac{1}{2}, -\frac{1}{2}\right) \right). \quad (\text{C.13})$$

- $m = +, n = t,$

$$= \left( \Gamma_2\left(+\frac{1}{2}, -\frac{1}{2}\right) H_+^i\left(+\frac{1}{2}, +\frac{1}{2}\right) H_t^{j*}\left(+\frac{1}{2}, -\frac{1}{2}\right) \right). \quad (\text{C.14})$$

- $m = +, n = 0,$

$$= \left( \Gamma_2\left(+\frac{1}{2}, -\frac{1}{2}\right) H_+^i\left(+\frac{1}{2}, +\frac{1}{2}\right) H_0^{j*}\left(+\frac{1}{2}, -\frac{1}{2}\right) \right). \quad (\text{C.15})$$

- $m = n = +,$

$$= \left( \Gamma_2\left(+\frac{1}{2}, +\frac{1}{2}\right) H_+^i\left(+\frac{1}{2}, +\frac{1}{2}\right) H_+^{j*}\left(+\frac{1}{2}, +\frac{1}{2}\right) \right). \quad (\text{C.16})$$

- $m = -, n = t,$

$$= \left( \Gamma_2\left(-\frac{1}{2}, +\frac{1}{2}\right) H_-^i\left(-\frac{1}{2}, -\frac{1}{2}\right) H_t^{j*}\left(-\frac{1}{2}, +\frac{1}{2}\right) \right). \quad (\text{C.17})$$

- $m = -, n = 0,$

$$= \left( \Gamma_2\left(-\frac{1}{2}, +\frac{1}{2}\right) H_-^i\left(-\frac{1}{2}, -\frac{1}{2}\right) H_0^{j*}\left(-\frac{1}{2}, +\frac{1}{2}\right) \right). \quad (\text{C.18})$$

- $m = n = -,$

$$= \left( \Gamma_2\left(-\frac{1}{2}, -\frac{1}{2}\right) H_-^i\left(-\frac{1}{2}, -\frac{1}{2}\right) H_-^{j*}\left(-\frac{1}{2}, -\frac{1}{2}\right) \right). \quad (\text{C.19})$$

The only non zero combination are  $m = +, n = -$  and  $m = -, n = +$ .

# Appendix D

## Related Formulae

In this section we have describe the formulae for wilson co-efficient and the form factor

### D.1 Wilson Coefficient

We provide the formulations of these Wilson coefficients, which we employed in our study, for the computation [10].

$$\begin{aligned}
 C_{\text{eff}}^7(q^2) &= C_7 - \frac{1}{3} \left( C_3 + \frac{4}{3}C_4 + 20C_5 + \frac{80}{3}C_6 \right) - \frac{\alpha_s}{4\pi} \left[ (C_1 - 6C_2)F_{1,c}^{(7)}(q^2) + C_8F_8^{(7)}(q^2) \right], \\
 C_{\text{eff}}^9(q^2) &= C_9 + \frac{4}{3} \left( C_3 + \frac{16}{3}C_5 + \frac{16}{9}C_6 \right) - h(0, q^2) \left( \frac{1}{2}C_3 + \frac{2}{3}C_4 + 8C_5 + \frac{32}{3}C_6 \right) \\
 &\quad - h(m_{\text{pole}}^b, q^2) \left( \frac{7}{2}C_3 + \frac{2}{3}C_4 + 38C_5 + \frac{32}{3}C_6 \right) \\
 &\quad + h(m_{\text{pole}}^c, q^2) \left( \frac{4}{3}C_1 + C_2 + 6C_3 + 60C_5 \right) \\
 &\quad - \frac{\alpha_s}{4\pi} \left[ C_1F_{1,c}^{(9)}(q^2) + C_2F_{2,c}^{(9)}(q^2) + C_8F_8^{(9)}(q^2) \right]. \tag{D.1}
 \end{aligned}$$

the functions are defined  $\text{ash}(m_{\text{pole}}^b, q^2)$  with  $q=c$ ,  $b$ , and functions  $F_8^{(7)}(q^2)$  are defined in [8], while the functions  $F_{2,c}^{(7,9)}(q^2)$  and  $F_{1,c}^{(7,9)}(q^2)$  are given in [7] for low  $s$  while for high  $s$  these formulae are given in [37].

### D.2 Form Factors

The parameterization in the "nominal fit" are

$$f(q^2) = \frac{1}{1 - \frac{q^2}{(m_{\text{pole}}^f)^2}} \left[ a_0^f + a_1^f z(q^2, t_+) \right]. \tag{D.2}$$

The parameterization in the "higher order fit" are

$$f(q^2) = \frac{1}{1 - \frac{q^2}{(m_{\text{pole}}^f)^2}} \left[ a_0^f + a_1^f z(q^2, t_+) + a_2^f (z(q^2, t_+))^2 \right], \tag{D.3}$$



where  $z(q^2, t_+)$  are defined as

$$z(q^2, t_+) = \frac{\sqrt{t_+ - q^2} - \sqrt{t_+ - t_0}}{\sqrt{t_+ - q^2} + \sqrt{t_+ - t_0}}, \quad (\text{D.4})$$

with  $t_+ = (m_{\Lambda_b} - m_{\Lambda})^2$  and  $t_0 = (m_B + m_K)^2$ . All masses and the values of the fit parameters for nominal fit and higher order fit are obtained from [4].

# Bibliography

- [1] A. Pich. The standard model of electroweak interactions. In *2010 European School of High Energy Physics*, pages 1–50, 1 2012.
- [2] Han Yan. Angular distribution of the rare decay  $\lambda_b \rightarrow \lambda(\rightarrow n\pi)\ell^+\ell^-$ . *arXiv preprint arXiv:1911.11568*, 2019.
- [3] Timo Aaltonen, B. Álvarez González, Silvia Amerio, D. Amidei, A. Anastassov, A. Annovi, J. Antos, G. Apollinari, J. A. Appel, A. Apresyan, et al. Observation of the baryonic flavor-changing neutral current decay  $\lambda_b^0 \rightarrow \lambda\mu^+\mu^-$ . *Physical Review Letters*, 107(20):201802, 2011.
- [4] William Detmold and Stefan Meinel.  $\lambda_b \rightarrow \lambda\ell^+\ell^-$  form factors, differential branching fraction, and angular observables from lattice qcd with relativistic b quarks. *Physical Review D*, 93(7):074501, 2016.
- [5] Diganta Das. On the angular distribution of  $\lambda_b \rightarrow \lambda(\rightarrow n\pi)\tau^+\tau^-$  decay. *Journal of High Energy Physics*, 2018(7):1–25, 2018.
- [6] Yu-Ming Wang, M. Jamil Aslam, and Cai-Dian Lü. Rare decays of  $\lambda_b \rightarrow \lambda\gamma$  and  $\lambda_b \rightarrow \lambda\ell^+\ell^-$  in the universal extra-dimension model. *The European Physical Journal C*, 59:847–860, 2009.
- [7] HH Asatryan, HM Asatrian, Christoph Greub, and M Walker. Calculations of two-loop virtual corrections to  $b \rightarrow s l^+ l^-$  in the standard model. *Physical Review D*, 65(7):074004, 2002.
- [8] Martin Beneke, Th Feldmann, and D Seidel. Systematic approach to exclusive  $b \rightarrow v^+ \ell^-$ ,  $v\gamma$  decays. *Nuclear Physics B*, 612(1-2):25–58, 2001.
- [9] Martin Beneke, Th Feldmann, and D Seidel. Exclusive radiative and electroweak and penguin decays at nlo. *The European Physical Journal C-Particles and Fields*, 41(2):173–188, 2005.
- [10] Faisal Munir Bhutta, Zhuo-Ran Huang, Cai-Dian Lü, M Ali Paracha, and Wenyu Wang. New physics in  $b \rightarrow s$  anomalies and its implications for the complementary neutral current decays. *Nuclear Physics B*, 979:115763, 2022.
- [11] Philipp Böer, Thorsten Feldmann, and Danny van Dyk. Angular analysis of the decay  $\lambda_b \rightarrow \lambda(\rightarrow n\pi)^+\ell^-$ . *Journal of High Energy Physics*, 2015(1):1–33, 2015.
- [12] Shibasis Roy, Ria Sain, and Rahul Sinha. Lepton mass effects and angular observables in  $\lambda_b \rightarrow \lambda(\rightarrow p\pi)\ell^+\ell^-$ . *Physical Review D*, 96(11):116005, 2017.
- [13] Quan-Yi Hu, Xin-Qiang Li, and Ya-Dong Yang. The  $\lambda_b \rightarrow \lambda(\rightarrow p\pi^-)\mu^+\mu^-$  decay in the aligned two-higgs-doublet model. *The European Physical Journal C*, 77:1–13, 2017.

- [14] Aneesh V Manohar. Effective field theory. *lectures at the Schlading Winter School*, 1996.
- [15] M Beneke. Effective field theory—concepts and applications. 2010.
- [16] Juan Rojo. The standard model effective theory: towards a pedagogical primer. *Phys. Rev. Lett. B*, 169, 2020.
- [17] Aneesh V Manohar and Mark B Wise. *Heavy quark physics*. Cambridge university press, 2000.
- [18] Michael E Luke, Aneesh V Manohar, and Ira Z Rothstein. Renormalization group scaling in nonrelativistic qcd. *Physical Review D*, 61(7):074025, 2000.
- [19] Stefan Scherer. Introduction to chiral perturbation theory. *Adv. Nucl. Phys.*, 27:277, 2003.
- [20] Christian W. Bauer, Sean Fleming, Dan Pirjol, and Iain W. Stewart. An Effective field theory for collinear and soft gluons: Heavy to light decays. *Phys. Rev. D*, 63:114020, 2001.
- [21] Andrea Quadri. Decoupling Limits in Effective Field Theories via Higher Dimensional Operators. 1 2024.
- [22] B. Grzadkowski, M. Iskrzynski, M. Misiak, and J. Rosiek. Dimension-Six Terms in the Standard Model Lagrangian. *JHEP*, 10:085, 2010.
- [23] Andrzej J Buras. Flavour dynamics: Cp violation and rare decays. In *Theory and Experiment Heading for New Physics*, pages 200–337. World Scientific, 2001.
- [24] Yosef Nir. Flavour physics and cp violation. *arXiv preprint arXiv:1010.2666*, 2010.
- [25] Yuval Grossman. Introduction to flavour physics. In *LHC Phenomenology*, pages 35–80. Springer, 2014.
- [26] Mark Thomson. *Modern Particle Physics*. Cambridge University Press, 2013.
- [27] Samoil M Bilenky and Jiří Hošek. Glashow-weinberg-salam theory of electroweak interactions and the neutral currents. *Physics Reports*, 90(2):73–157, 1982.
- [28] Demosthenes Kazanas. Dynamics of the universe and spontaneous symmetry breaking. *The Astrophysical Journal*, 241:L59–L63, 1980.
- [29] Andrzej J Buras. Weak hamiltonian, cp violation and rare decays. *arXiv preprint hep-ph/9806471*, 1998.
- [30] Stefan Hollands and Robert M. Wald. The Operator Product Expansion in Quantum Field Theory. 12 2023.
- [31] Robert Fleischer. Cp violation and the role of electroweak penguins in nonleptonic b decays. *International Journal of Modern Physics A*, 12(14):2459–2522, 1997.
- [32] Amand Faessler, Thomas Gutsche, M. A. Ivanov, J. G. Körner, and Valery E. Lyubovitskij. The exclusive rare decays  $b \rightarrow k^{(*)} \ell^+ \ell^-$  and  $k \rightarrow \pi \ell^+ \ell^-$  in a relativistic quark model. *EPJ direct*, 4(1):1–33, 2002.
- [33] Fulvia De Fazio, Thorsten Feldmann, and Tobias Hurth. Scet sum rules for  $b \rightarrow p$  and  $b \rightarrow v$  transition form factors. *Journal of High Energy Physics*, 2008(02):031, 2008.
- [34] Marcel Algueró, Aritra Biswas, Bernat Capdevila, Sébastien Descotes-Genon, Joaquim Matias, and Martín Novoa-Brunet. To (b) e or not to (b) e: No electrons at lhcb. *arXiv preprint arXiv:2304.07330*, 2023.

- [35] Luca Silvestrini. Effective theories for quark flavour physics. *arXiv preprint arXiv:1905.00798*, 2019.
- [36] Kresimir Kumericki. Feynman diagrams for beginners. *arXiv preprint arXiv:1602.04182*, 2016.
- [37] C. Greub, V. Pilipp, and C. Schüpbach. Analytic calculation of two-loop qcd corrections to  $b \rightarrow s\ell^+\ell^-$  in the high  $q^2$  region. *Journal of High Energy Physics*, 1:1–40, 2008.